





3 | Molecular and Cellular Biology | Research Article

Physiology, fast and slow: bacterial response to variable resource stoichiometry and dilution rate

Logan M. Peoples, 1 Jana Isanta-Navarro, 1.2 Benedicta Bras, 1 Brian K. Hand, 1 Frank Rosenzweig, 3.4 James J. Elser, 1 Matthew J. Church 1

AUTHOR AFFILIATIONS See affiliation list on p. 15.

ABSTRACT Microorganisms grow despite imbalances in the availability of nutrients and energy. The biochemical and elemental adjustments that bacteria employ to sustain growth when these resources are suboptimal are not well understood. We assessed how Pseudomonas putida KT2440 adjusts its physiology at differing dilution rates (to approximate growth rates) in response to carbon (C), nitrogen (N), and phosphorus (P) stress using chemostats. Cellular elemental and biomolecular pools were variable in response to different limiting resources at a slow dilution rate of 0.12 h⁻¹, but these pools were more similar across treatments at a faster rate of 0.48 h⁻¹. At slow dilution rates, limitation by P and C appeared to alter cell growth efficiencies as reflected by changes in cellular C quotas and rates of oxygen consumption, both of which were highest under P- and lowest under C- stress. Underlying these phenotypic changes was differential gene expression of terminal oxidases used for ATP generation that allows for increased energy generation efficiency. In all treatments under fast dilution rates, KT2440 formed aggregates and biofilms, a physiological response that hindered an accurate assessment of growth rate, but which could serve as a mechanism that allows cells to remain in conditions where growth is favorable. Our findings highlight the ways that microorganisms dynamically adjust their physiology under different resource supply conditions, with distinct mechanisms depending on the limiting resource at slow growth and convergence toward an aggregative phenotype with similar compositions under conditions that attempt to force fast growth.

IMPORTANCE All organisms experience suboptimal growth conditions due to low nutrient and energy availability. Their ability to survive and reproduce under such conditions determines their evolutionary fitness. By imposing suboptimal resource ratios under different dilution rates on the model organism *Pseudomonas putida* KT2440, we show that this bacterium dynamically adjusts its elemental composition, morphology, pools of biomolecules, and levels of gene expression. By examining the ability of bacteria to respond to C:N:P imbalance, we can begin to understand how stoichiometric flexibility manifests at the cellular level and impacts the flow of energy and elements through ecosystems.

KEYWORDS resource limitation, growth rate, bacteria, transcriptomics, stoichiometry, *Pseudomonas putida*

S toichiometric imbalances occur in microorganisms when the proportions of elements available for their growth (e.g., Carbon:Nitrogen:Phosphorus; C:N:P) differ from those optimal for biomass synthesis and metabolism. Such imbalances can have consequences for the flow of elements and energy through ecosystems, potentially lowering trophic efficiencies and influencing nutrient cycling (1, 2). Deviations in the proportions or concentrations of growth-requiring elements relative to cellular demands can result in energy or nutrient limitation of population sizes (*Liebig* limitation) or growth

Editor Lennart Schada von Borzyskowski, Universiteit Leiden, Leiden, Netherlands

Address correspondence to Logan M. Peoples, logan.peoples@flbs.umt.edu.

The authors declare no conflict of interest.

See the funding table on p. 16.

Received 6 June 2024 Accepted 19 June 2024 Published 9 July 2024

Copyright © 2024 Peoples et al. This is an openaccess article distributed under the terms of the Creative Commons Attribution 4.0 International license.

10.1128/msystems.00770-24 2

Research Article mSystems

rates (*Blackman* limitation) (3–5). Such resource (energy and nutrient) limitations can cause dramatic alterations in organismal physiology, including changes in elemental stoichiometry, biochemical composition, and gene transcription (6, 7). Here, we use the more general term *stress* to describe the pressure imposed by imbalanced resource ratios while making no inherent assumptions about changes in physiology.

The physiology of an organism is dependent on its rate of growth. The tipping point that defines the transition between when one resource becomes limiting relative to another can vary with growth rate (8). At slow growth rates, heterotrophic bacteria vary their biomass stoichiometry in response to changes in resource stoichiometry, including C:N:P ratios and macromolecular composition (9–11). By contrast, when organisms approach their maximal growth rates (μ_{max}), biomass stoichiometry shows less variability despite differences in resource supply ratios (12–14). To explain such observations, Monod reasoned that as an organism approaches its maximum growth rate, all cellular reactions operate at some optimal rate, leading to convergence in the composition of cellular elemental and macromolecular pools (15). However, the mechanisms underlying how bacteria modulate cellular physiology in response to both resource stress and growth rate are not well explored.

The genus *Pseudomonas* is taxonomically diverse, near ubiquitous in its distribution, and remarkable for its capacity to adjust to different environments (16–18). One of the most well-studied pseudomonads is *Pseudomonas putida* KT2440 (19, 20). KT2440 is known for its broad metabolic versatility and genetic plasticity, generating interest in its ability to cope with environmental stress as well as its biotechnological potential (21, 22). The physiology of this organism has been thoroughly studied, including through the creation of whole-genome sequences and metabolic models (23–25). KT2440 responds dynamically to nutrient limitation through changes in gene expression and energy storage (26–28). Moreover, under nutrient-replete conditions that promote rapid growth, *P. putida* can form biofilms that subsequently disperse at the onset of nutrient starvation (29–31). To date, less is known about the mechanisms underlying how KT2440 responds to the interplay between resource stoichiometry and growth rate.

Here, we used *P. putida* KT2440 as an experimental model to gain insight into the flexibility of cell physiology in the face of resource stress. We asked (i) How does variable resource stoichiometry impact biomass stoichiometry and metabolic activity? and (ii) How does bacterial physiology change as a function of growth rate? To answer these questions, we cultured KT2440 in chemostats at both relatively slow (0.12 h⁻¹) and fast (0.48 h⁻¹) dilution rates with media resource stoichiometry designed to facilitate balanced growth or to promote carbon (C), nitrogen (N), or phosphorus (P) stress. At slow dilution rates, we observed physiological changes that varied as a function of resource stoichiometry, including those linked to carbon and energy flow and storage. At high dilution rates cells aggregated, complicating chemostat dynamics, but in all treatments demonstrated similar biochemical and transcriptome responses despite differing resource supply ratios. Our study highlights the effects of elemental stoichiometry and growth rate on bacterial physiology and provides insight into the mechanisms required to sustain growth in the face of imbalanced resource ratios.

MATERIALS AND METHODS

Media composition

Pseudomonas putida KT2440 (DSM 6125) was grown in a modified version of COMBO medium originally developed for the growth of aquatic zooplankton and phytoplankton (32). Normal culture conditions included 200 mM C as glucose (33.3 mM), 10 mM N as NH₄Cl, and 0.625 mM P as K₂HPO₄, yielding a C:N:P molar ratio of 320:16:1. We refer to this medium as "Balanced" throughout the manuscript as it (i) reflects an N:P of typical organismal biomass (11, 33–35) and (ii) has a C:P ratio near the boundary between C- and P- deficient conditions of some bacteria (36). The medium was buffered with 40 mM HEPES to a final pH of 7.4. The medium was prepared by first autoclaving CaCl₂

August 2024 Volume 9 Issue 8

and Fe:EDTA dissolved in high-purity water (18.2 mega-ohm); this was cooled and a concentrated preparation of all remaining components, which had been filter-sterilized through a 0.2 μ m polyethersulfone filter, was aseptically amended (Table S1).

C:N:P ratios in COMBO medium were manipulated to impose resource stress by decreasing the concentration of one element from Balanced medium conditions. Based on results from batch culture experiments (Fig. S1), C:N:P molar ratios used for the chemostats were 320:16:1 (Balanced), 40:16:1 (C-stress), 320:6:1 (N-stress), and 320:16:0.2 (P-stress). These elemental ratios are consistent with those previously observed to force resource stress in aquatic bacteria beyond a typical biomass C:N:P of ~70:16:1 (11, 35).

Growth conditions

KT2440 was grown in chemostats at 20°C with a culture volume of 75 mL (37, 38). Cultures were grown at two different dilution rates to represent slow and fast growth: 0.12 h^{-1} and 0.48 h^{-1} . The maximum specific growth rate at 20°C under batch culture conditions exceeded 0.5 h^{-1} (Fig. S1), and empirical observations in chemostats showed that planktonic KT2440 washed out at dilution rates exceeding 0.6 h^{-1} but not at 0.48 h^{-1} . Hence, a dilution rate of 0.48 h^{-1} approached the maximum growth rate for this organism at 20°C. Previously reported maximum growth rates for KT2440 average ~0.6 h^{-1} at 30°C (27, 39, 40).

To initiate all experiments, a cryo-preserved glycerol (20% vol/vol) stock of KT2440 was streaked onto an LB agar plate (BD Difco, Thermo Fisher Scientific, USA) and incubated at 20°C. A single colony was picked, inoculated in Balanced COMBO medium, and incubated overnight with shaking. One mL of stationary-phase culture was inoculated into each chemostat and incubated overnight in batch mode. Each resource stress treatment was performed in quadruplicate chemostats. After each chemostat became turbid, chemostats were switched from batch to continuous culture with the dilution rate controlled using a peristaltic pump (Watson-Marlow 205S, 16 channel). For the low dilution rate, the flow rate was immediately set to 0.12 h⁻¹, while for the high dilution rate (0.48 h⁻¹) the chemostat flow rates were increased stepwise over a 24-h period. Oxygen (O₂) was controlled using aquarium pumps and, in fully turbid cultures, was sustained at 150 μ M (equivalent to ~55% saturation). The chemostat pH ranged between 6.5 and 7. Chemostats were sampled after cells reached steady state (five residence times at the appropriate dilution rate (41)).

Sampling constraints

To sample chemostats, the entire culture volume was removed and immediately processed for downstream analyses. Cell aggregation (flocculation) was observed in all treatments at dilution rates exceeding 0.3 h⁻¹ (see Results and Discussion). Cells were observed to disaggregate approximately 1 h after being removed from the chemostat. Therefore, all assays described below were completed within 30 minutes of sampling to minimize physiological changes. We acknowledge that this sampling interval may bias our results and interpretation.

Residual nutrient quantification

The residual concentrations of media N and P remaining in each chemostat were quantified. The inflow medium (~20 mL) was filtered through a rinsed, 0.45 μ m pore size, mixed cellulose ester (MCE) filter. Prior to the disassembly of each chemostat for sampling, equal volumes of culture outflow (~5 mL) from each chemostat treatment were pooled (~20 mL) and filtered as above. Filtrate was stored at -20° C. Ammonium (NH₄⁺) and soluble reactive phosphorus (SRP) were quantified using an Astoria A2 segmented flow analyzer (Astoria-Pacific, OR, USA). The percent concentrations of residual NH₄⁺ and SRP were calculated by dividing the N or P remaining in the outflow by the initial concentrations in the media. Because the outflow from each chemostat treatment was pooled, values represent averages of four replicate chemostats per treatment.

Biomass determinations: Dry weight, cell counts, cell volumes, and ATP

To estimate biomass dry weight, chemostat culture (10 mL) was filtered onto a preweighed 25 mm diameter 0.2 µm GTTP polycarbonate filter (MilliporeSigma). The filter was dried at 105°C overnight, stored in a desiccator, and reweighed. Cell abundances were estimated by epifluorescence microscopy of DAPI-stained bacteria. One mL of culture was fixed with a final concentration of 3% formaldehyde overnight at 4°C. Cells were filtered onto a 25 mm, 0.2 µm GTTP filter, and frozen at -20°C. DNA was stained using DAPI Vectashield (Vector Laboratories) and cells were visualized using an epifluorescence microscope (Olympus BX53) at 1,000× magnification. At least 10 fields of view or 200 cells were counted per sample. Cell volumes were estimated assuming the cell shape was a spherocylinder (42). Adenosine triphosphate (ATP) concentrations were determined via luminescence production using the BacTiter-Glo Microbial Cell Viability Assay (Promega, WI, USA). Briefly, 100 μL of culture was mixed with an equal volume of BacTiter-Glo reagent and incubated in the dark at room temperature for 5 min. Luminescence was quantified using a luminometer (GloMax 20/20, Promega). ATP concentrations were calculated based on a standard curve made from ATP disodium salt (Sigma-Aldrich, MA, USA).

Cellular phosphorus

To measure cell phosphorus content, 3 mL of chemostat culture was filtered onto a pre-combusted, acid-washed, 25 mm, 0.7 μ m glass fiber filter (Whatman). Filters were dried overnight at 105°C and stored in a desiccator. Filters were then placed in a scintillation vial and combusted at 500°C for 5 h. Samples were hydrolyzed with 10 mL of 0.15 M HCl at 60°C for 1 h. Finally, samples were treated with ammonium molybdate and potassium antimonyl tartrate, which, in the presence of ascorbic acid, allows for the quantification of phosphorus (43).

Cellular carbon and nitrogen

Particulate C and N contents were determined from a set of chemostats run in parallel that were sacrificed specifically for these measurements to obtain sufficient biomass. Approximately 50 mL of culture was centrifuged at $4,300 \times g$ for 10 min at 4°C. The cell pellet was washed with high-purity water (18.2 mega-ohm), centrifuged, and the supernatant discarded. This was repeated three times. The cell pellet was dried overnight at 105° C, stored in a desiccator, and weighed. The C and N contents were determined using an Exeter Analytical CE-440. C:N, N:P, and C:P ratios are reported as averages of the means with standard error uncertainty propagation.

Concentrations of DNA and RNA

DNA and RNA were quantified fluorometrically as previously described (44, 45) using the Quant-iT Ribogreen RNA Reagent and Kit (Thermo Fisher Scientific). One mL of culture was centrifuged at 22,000 \times g for 10 min at 4°C. The supernatant was discarded and the cell pellet was frozen at -80° C. The pellet was resuspended in 300 μ L of extraction buffer (1% N-lauroylsarcosine in 1× TE buffer), sonicated on ice for 2 min, and incubated for 2 h with shaking at room temperature. Samples were diluted 1:6 with ice-cold Tris-EDTA buffer and incubated for 15 min with agitation. Samples (75 μ L) were added to a 96-well black microplate, amended with 75 μ L Ribogreen, and incubated for 5 min in the dark. Fluorescence was measured at 485/30 nm excitation and 528/20 emission on a microplate reader (FLx800 Bio-Tek). Samples were then amended with 10 μ L of RNAse (Promega) to remove RNA, incubated in the dark for 25 min, and fluorescence was remeasured. RNA and DNA concentrations were calculated based on the difference in fluorescence against a set of RNA and DNA standards.

Lipids

Lipid contents were determined using previously described methods (46–48). One mL of culture was centrifuged, freeze-dried, and stored at –80°C. The lyophilized culture was homogenized in a 2:1 chloroform:methanol mixture and extracted using the microsulfophosphovanillan method. Standards were prepared by dissolving cholesterol in 2:1 chloroform:methanol. Samples and standards were read on a spectrophotometer (Agilent Cary 60 UV-Vis) at 525 nm.

Protein

Total protein quantification was performed using the Thermo Scientific Coomassie Plus Kit (Thermo Fisher Scientific). One mL of culture was pelleted at 22,000 \times g for 5 min and frozen at -80° C. The pellet was homogenized in 400 μ L 30% trichloroacetic acid, incubated at 4°C for 30 min, and then centrifuged at 15,500 \times g at 4°C for 10 min. After the supernatant was removed, the pellet was rinsed with 5% TCA, treated with 300 μ L of 0.2 M sodium hydroxide (NaOH), and vortex homogenized. Each sample (50 μ L) was amended with 1.5 mL of Coomassie Plus Reagent (Thermo Fisher Scientific) and incubated for 10 min at room temperature. Protein content was determined colorimetrically at 595 nm on a spectrophotometer against protein standards ranging from 25 to 2000 μ g mL⁻¹.

Oxygen consumption

Chemostat culture (15 mL) was diluted with 150 mL of the appropriate medium and immediately placed into a glass serum bottle equipped with an Oxygen Sensor Spot optode (PreSens). Optodes were affixed to the inside of the bottles and fiber optic cables were attached to the outside for light excitation and detection of emission. Bottles were crimp-sealed and O_2 concentrations were measured in the dark over 20 min to estimate rates of consumption. Cultures were diluted into fresh media because respiration rates were faster than our ability to set up the experiment before O_2 was completely consumed (e.g., 5 min). As our measurements were made following the dilution of cells into fresh media, they likely reflect an upper limit on rates of O_2 consumption for each treatment.

Transcriptomic sequencing

Culture (\sim 15 mL) from each of four replicate chemostats was centrifuged at 4,300 \times g for 10 min at 4°C and the supernatant was discarded. The cell pellet was submerged in RNAlater (Thermo Fisher Scientific) and stored at -20°C. Total RNA was extracted using the RNeasy Mini Kit (Qiagen, Germany). RNA library preparation, rRNA depletion, and sequencing on an Illumina Novaseq were performed using protocols recommended by the manufacturers (Novogene, Inc., Sacramento, CA).

Raw reads were cleaned with Trimmomatic v0.39 (49). Read recruitment against the KT2440 genome (NCBI accession GCA_000007565; 23, 50) was performed using Bowtie 2 v2.3.5.1 (51) and SAMtools v1.10 (52). Recruitment against each gene was quantified using featureCounts (53). Functional annotation was performed using NCBI Prokaryotic Genome Annotation Pipeline annotations (54) and GhostKOALA (55) against the KEGG database (56). Reads that mapped to ribosomal RNA genes were removed from further analysis. Gene expression was normalized using the metric Transcripts Per Million (TPM) for comparison and visualization. To show transcriptional differences of multiple treatments at the same time, we averaged the TPM of each gene across replicates within a given treatment and then normalized its expression relative to other treatments using the R package GGtern (57). We compared treatments using NMDS ordinations based on Bray-Curtis dissimilarities of rarefied recruitment counts with vegan (58). We tested whether resource stoichiometry and dilution rate were statistically significant drivers of transcriptome composition using *adonis* in vegan. DESeq2 (59) was used on unrarefied gene counts to identify differentially expressed genes between different

resource stresses and dilution rates. To identify potential pathways that were differentially expressed, genes were grouped into functional categories based on KEGG pathway annotations using KEGGREST (60). Figures were made using ggplot2 (61) and BioRender (https://biorender.com/).

RESULTS

Elemental and biomolecular pools

We assessed the physiological response of *P. putida* KT2440 to differences in resource stoichiometry and chemostat dilution (growth) rate based on measurements of elemental and biochemical pools, cell morphology, O_2 consumption, and transcriptome composition. Dry weight yield was greatest (0.5 g L⁻¹) in the Balanced treatment and lowest in the P-stressed treatment (0.2 g L⁻¹) at both dilution rates (Fig. S2). Cell abundance at 0.12 h⁻¹ (slow dilution) was typically 3×10^8 cells mL⁻¹ under all conditions except P-stress, where cell densities were ~1 $\times 10^8$ cells mL⁻¹. Dry weight cell⁻¹ and volume cell⁻¹ at 0.12 h⁻¹ were lowest in the C-stressed treatment (Student's *t*-test, C vs Balanced, P < 0.05), while ATP dry weight⁻¹ was highest under C- and lowest under P-stress (C vs P, $P < 1 \times 10^{-4}$). However, ATP cell⁻¹ was largely invariant across treatments at the slow dilution rate (averaging ~2 $\times 10^{-9}$ nmol cell⁻¹; ANOVA, P < 0.61), consistent with ATP concentrations reflecting cytoplasm volume rather than biomass *per se* (62).

One of the most obvious phenotypic shifts that accompanied increases in dilution rate was cell autoaggregation and biofilm formation. At a dilution rate of 0.48 h⁻¹ cells tended to clump, forming visually apparent aggregates containing hundreds of cells with combined lengths that could exceed 70 µm. This behavior was evident across all resource ratios and prevented accurate enumeration of cell abundances. Visual observation showed that cells released from aggregates after 1 h of removal from the chemostat. The tendency to aggregate and form biofilms complicates the assessment of growth rate; previous studies have found that cells within aggregates and biofilms can grow at different rates (63, 64), which in chemostats may violate the assumption of steady-state behavior. The increase in dilution rate clearly triggered a phenotypic response (cell aggregation), but it remains unclear the extent to which the cells in these high dilution treatments were uniformly growing at the specified growth rate (0.48 h⁻¹) or whether the aggregation response resulted in a mixed population of fast and slow growing cells. Given this uncertainty, we refer to the dilution rate rather than the growth rate when comparing treatments.

For each treatment, we measured cellular C, N, and P contents (Fig. 1). Together, these three elements accounted for ~50%-60% of the observed KT2440 dry weight. At the slow dilution rate, carbon accounted for a smaller proportion of the dry weight when cells were grown under C-stressed conditions, while cells became increasingly carbonrich and larger under P-stressed conditions, representing ~43% and 48% of the dry weight, respectively (C vs. P, P < 0.042). By contrast, dry weight-normalized N contents were lowest under P- and N-stress and greatest under C-stress, ranging between ~9.5% and 12.5% (C vs. P, P < 0.07). P accounted for a significantly lower fraction ($\sim 0.6\%$) of the dry weight under P-stress than the other treatments at the slow dilution rate. As a result, C:N, C:P, and N:P molar ratios were highest under P- (~5.9, 236, 40, respectively) and lowest under C- (~4.5, 93, 21) stress. Elemental contents and ratios in the Balanced medium treatment, which was intended to represent optimal resource ratios for growth, generally fell between values observed in the N- and P-stressed treatments. At the faster dilution rate, C, N, and P contents per unit dry weight and the resulting molar ratios were more similar among treatments: for example, C, N, and P contents in all treatments averaged 45%, 12%, and 1.6%, respectively, while the C:N, C:P, and N:P ratios averaged 4.2, 70, and 15, indicating average biomass C:N:P of ~70:15:1. Coefficient of variation of resource ratios within all treatments decreased with increasing dilution rate (C:N, 0.11 to 0.07; C:P, 0.41 to 0.24; N:P, 0.32 to 0.27).

We also measured cellular pools of protein, lipid, RNA, DNA, and ATP (Fig. S3). Together, these macromolecular pools represented ~45%–60% of the dry weight. At the

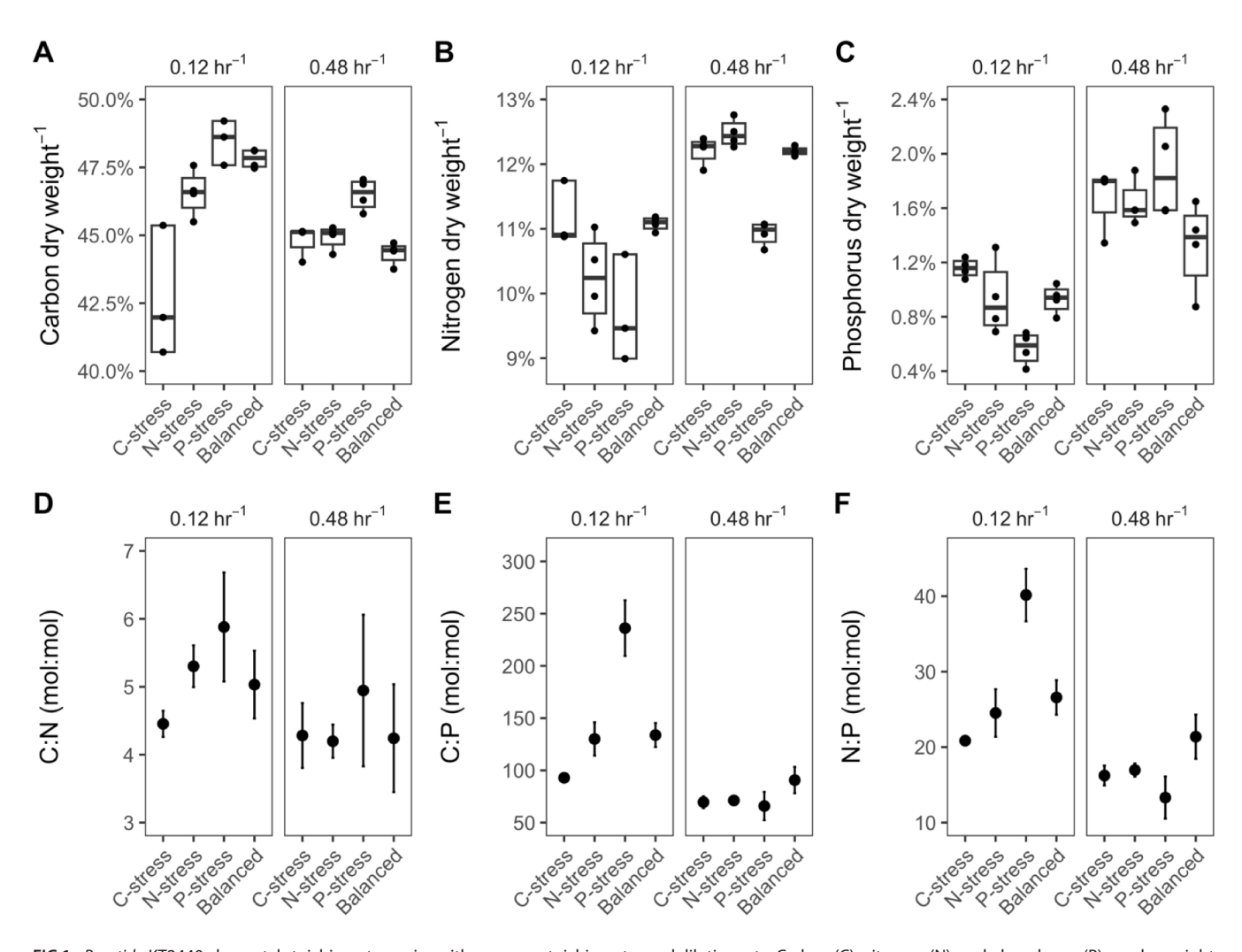


FIG 1 *P. putida* KT2440 elemental stoichiometry varies with resource stoichiometry and dilution rate. Carbon (C), nitrogen (N), and phosphorus (P) per dry weight (A, B, C) and their molar ratios (D, E, F). Note that Y-axes are not the same across plots.

slow dilution rate, protein represented 14%–25% of the dry weight, with P-stressed cells demonstrating the lowest protein content, while C-stressed treatments demonstrated elevated protein content. Protein content increased (23%–30% of dry weight) with dilution rate across all treatments (t-test, $P < 1 \times 10^{-5}$). Total lipids exhibited opposite patterns. At slow dilution rates, the lipid content of C-stressed cells was lowest (14%), while P-stressed cells were enriched in lipids (25% dry weight; C vs P, t-test, $P < 1 \times 10^{-3}$). Across all resource treatments, lipid content decreased at faster dilution rates (0.12 h⁻¹ vs 0.48 h⁻¹, t-test, P < 0.02). RNA content represented ~10% of the biomass and increased with dilution rate in all treatments except Balanced conditions (t-tests, P < 0.05). Cells under P-stress showed the most dramatic changes in RNA with dilution rate, increasing from 3% of the dry weight at 0.12 h⁻¹ to 10% at 0.48 h⁻¹. DNA and ATP represented small proportions of the dry weight under all conditions, comprising <3% and <0.13%, respectively. Similar to elemental content and stoichiometry, macromolecular content per dry weight converged at a higher dilution rate regardless of media resource composition.

Slow-growing cells adjust their physiology to acquire the limiting resource

We used transcriptomic sequencing for mechanistic insights into the adaptive strategies of KT2440 in response to variations in resource stoichiometry and dilution rate. When

comparing transcriptomes of cells cultured at $0.12\ h^{-1}$, the type of resource stress was a statistically significant predictor of transcriptome composition (PERMANOVA, $R^2=0.747$, P<0.001). There were 2,576, 1,139, and 1,847 differentially expressed genes when comparing C- and P-, C- and N-, and N- and P- stressed treatments, respectively (Tables S2 to S8), indicating that, at a fixed dilution rate, different kinds of resource stress induce distinct patterns of transcription. The most differentially expressed genes among treatments were involved in the uptake and assimilation of whichever resource was limiting, including glucose, ammonium, and phosphate (Fig. 2). These transcripts were likely controlled by increased expression of key regulatory pathways. For example, under C-stress, KT2440 expressed the non-protein-coding RNAs crcZY to sequester the Crc protein, thereby inhibiting carbon catabolite repression and releasing genes

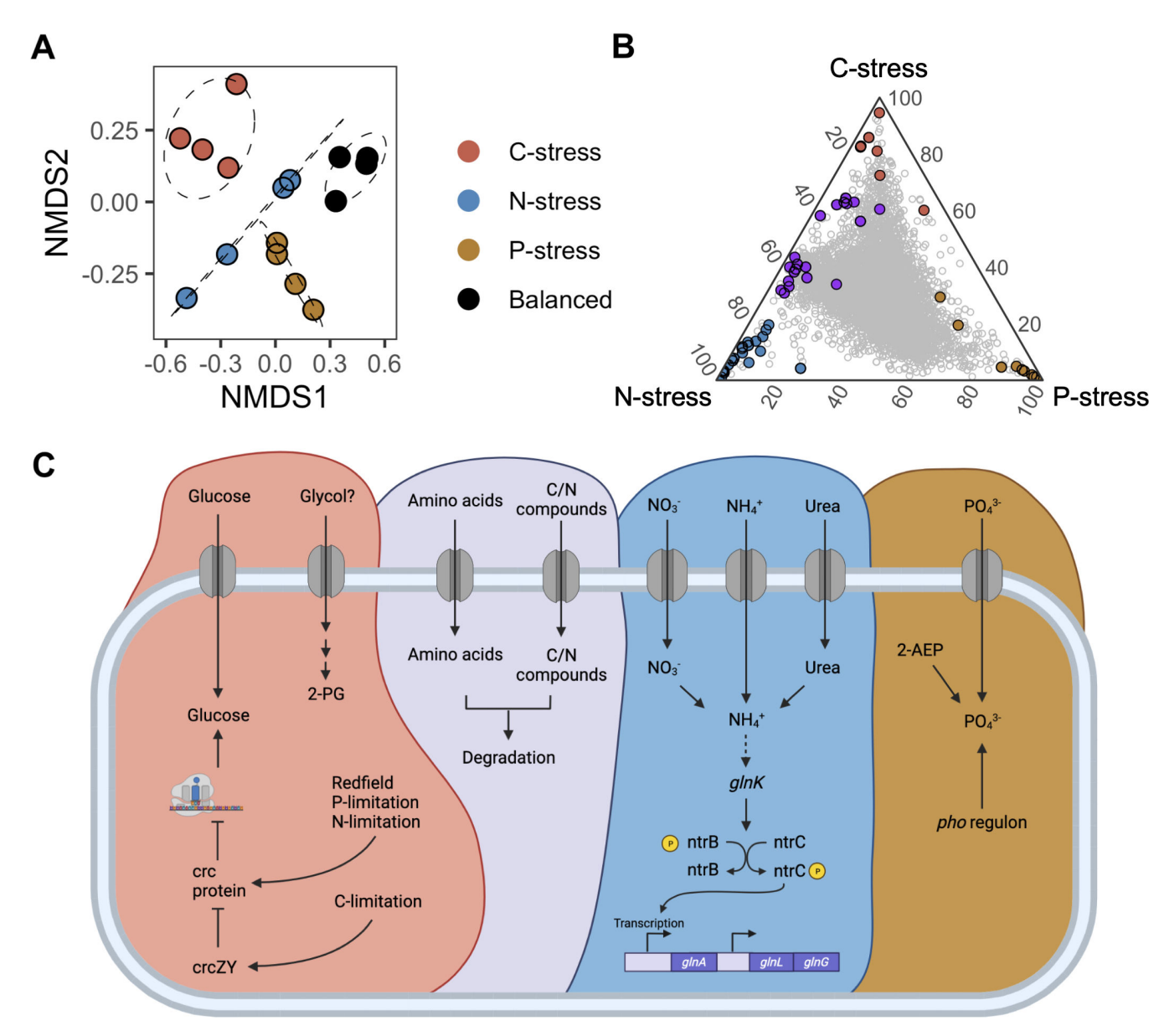


FIG 2 The major transcriptional response to variable resource stoichiometry at a dilution rate of 0.12 h⁻¹ (slow growth) is the expression of genes to obtain the limiting resource and their global regulators. (A) Non-metric multidimensional scaling (NMDS) ordination based on Bray-Curtis dissimilatory of transcriptomes. Circles represent the 75% confidence interval for each resource ratio. (B) Ternary plot comparing average relative percent transcript expression between C-, N-, and P-stressed resource treatments, where each gray circle represents a gene. Genes of interest are shown in color. (C) Cartoon highlighting major pathways involved in nutrient uptake and global regulation within each treatment. The colors in A, B, and C are the same; for example, the genes enriched under C-stress are red in all panels. Genes in purple in B and C are shared under C- and N- stress.

for glucose assimilation (65-67). Under N- and P-stress, respectively, the gln and pho regulons were highly expressed, operons that function in sensing and responding to N and P deficiency (26, 68). Interestingly, KT2440 also expressed transcripts that encode proteins for the uptake of C, N, and P in forms that were not provided in the media. For example, C-stressed cells transcriptionally expressed a putative porin involved in the uptake of ethylene glycol (69), N-stressed cells expressed genes for the transport of nitrate and urea and their conversion to ammonium before assimilation, while P-stressed cells transcribed phnXW whose products function in the degradation of 2-aminoethylphosphonate. Furthermore, cells in some treatments shared expression of transcripts that were largely absent in the remaining treatment. For example, under C- and N-stress, transporters involved in the uptake and degradation of compounds that had both C and N moieties, such as amino acids, were expressed. By contrast, transcripts for the synthesis and turnover of RNA and proteins were elevated in the N- and P-stressed treatments relative to C-stress, including elongation factor P, an endonuclease, a polyribonucleotide nucleotidyltransferase, and a putative protease (26). Relatively, fewer transcripts were shared by C- and P-stressed cells.

Central carbon metabolism and energy flux

Given differences in biomass C content between treatments, we assessed pathways involved in central C metabolism. Transcripts involved in glucose catabolism and the tricarboxylic acid (TCA) cycle (70) were more highly expressed under P- and N- relative to C-stress (Fig. S4). Transcripts involved in fatty acid biosynthesis and degradation, along with genes that function in the synthesis, structure, and degradation of polyhydroxyalkanoates (PHAs) were especially enriched under P-stress. The general trend toward higher relative expression of these pathways under P-stress was maintained even at fast dilution rates, consistent with elevated C:P ratios and lipid contents of these cells.

Differences in C metabolism would be expected to have ramifications for energy generation, respiratory O_2 consumption, and growth efficiency. When normalized to dry weight, rates of O_2 consumption were lowest in slow dilution rate P-stressed cells (C vs P, P < 0.01); however, when normalized to ATP (or per cell), C-stressed cells demonstrated the lowest rates of respiration (Fig. 3; C vs P, $P < 1.7 \times 10^{-3}$). Here again, we leveraged the transcriptome for potential clues into the underlying cause of these metabolic differences. The five terminal oxidases involved in the electron transport chain showed resource-stress-specific differences in expression at slow growth (Fig. S5). C-stressed cells expressed the aa_3 oxidase and to a smaller extent cio, while the cbb_3 -1 oxidase was more highly expressed under P-stress. Transcripts encoding proteins that catalyze the first step of electron transfer and final step of ATP generation, such as nuo dehydrogenase, succinate dehydrogenase, and ATP synthase, were less abundant under C-stress. These observations indicate that C-stress alters energy-generating pathways.

Dilution-rate-dependent responses

NMDS ordination analysis based on Bray-Curtis dissimilarity showed that transcriptome composition across all treatments was less variable at a dilution rate of 0.48 h⁻¹ relative to 0.12 h⁻¹ (Fig. 4). Resource stoichiometry was a weaker predictor of transcript composition at the higher dilution rate relative to the slow dilution rate (R² = 0.473, P < 0.024). When comparing all treatments together, both dilution rate and resource stoichiometry were statistically significant drivers of transcriptome composition (dilution rate, R² = 0.11, P < 0.002; resource stoichiometry, R² = 0.38, P < 0.001). Over 2,000 genes were differentially expressed between the slow and fast dilution rate treatments (Table S9). Many important metabolic genes that were differentially expressed at slow dilution rates, including those involved in cellular respiration, glucose catabolism, and the TCA cycle, did not differ as a function of resource stress at the faster dilution rate (Fig. S6). Nevertheless, even at fast dilution rates, cells in the P- and N-stressed treatments overexpressed transcripts for proteins involved in the transport and assimilation of P and N, respectively.

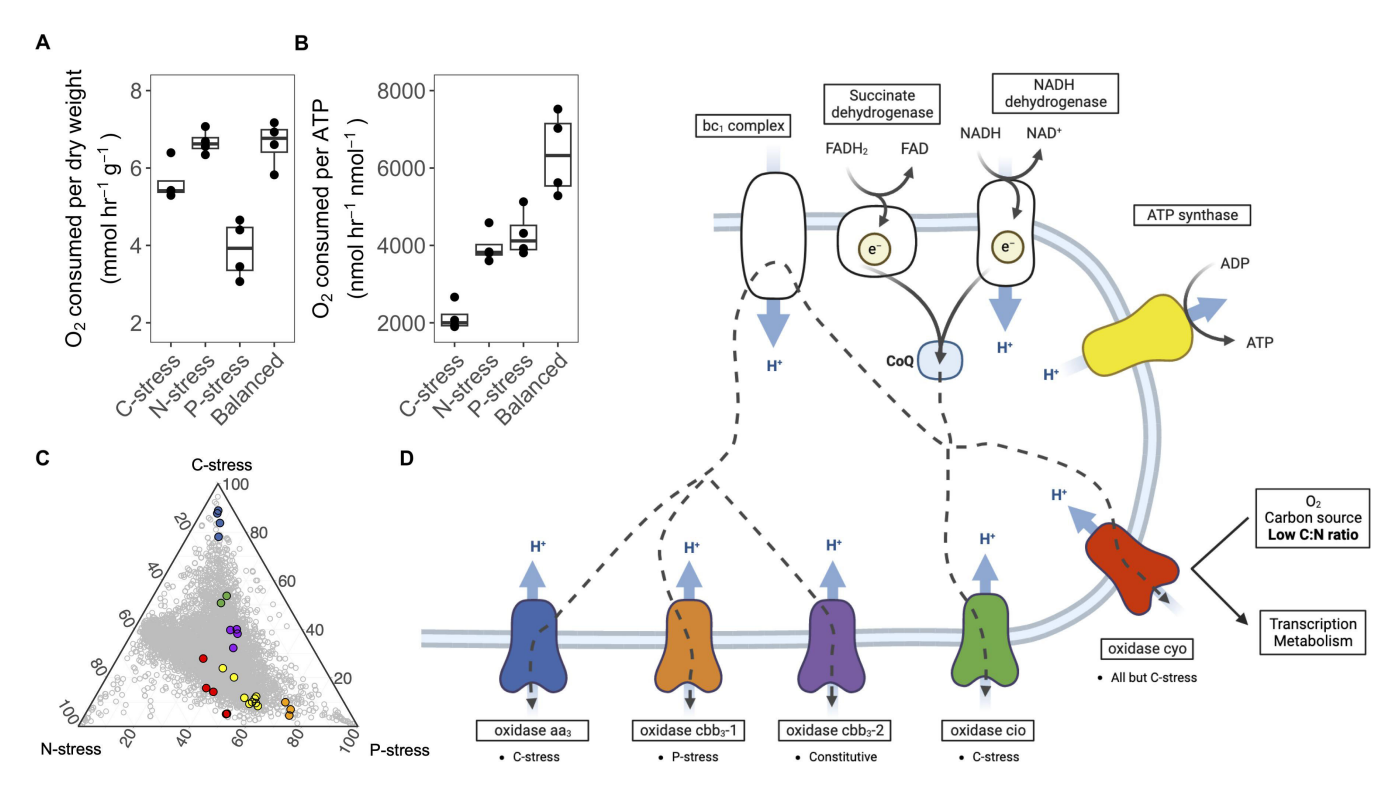


FIG 3 Respiratory changes appear critical to adaptation to variable resource stoichiometry at a dilution rate of 0.12 h⁻¹. (A and B) Oxygen consumption per dry weight and per ATP. Note that Y-axes are not the same between plots. (C) Ternary plot comparing relative percent transcript expression between C-, N-, and P-limited resource ratios at 0.12 h⁻¹, where each gray circle represents a gene. Respiratory genes of interest are represented in color. (D) A cartoon of the electron transport chain of *P. putida* KT2440. The colors of the terminal oxidases and ATP synthase in panel D reflect the genes in C.

When comparing transcriptomes at fast versus slow dilution rates, some of the most differentially abundant genes included those associated with ribosomes. When grouping genes based on KEGG pathways, those involved in the synthesis of ribosomal proteins, tRNA biosynthesis, amino acid biosynthesis, and DNA replication were more highly expressed in cells at fast than at slow growth (Fig. 4). These changes were especially evident under P-stress and more modest for C- and N-stress, largely consistent with treatment-specific differences in biomass P and RNA content. For example, under N-stress, no ribosomal protein genes were differentially expressed at the faster dilution rate relative to the slower one (Fig. S7). The RNA to protein ratio, which is known to increase with growth rate (71–74), increased with dilution rate under P-stress and balanced conditions but not in C- or N-stressed cells. Departures from the expected increase in the RNA:protein ratio with growth rate could reflect the storage of ribosomes under slow growth conditions. Consistent with this idea, the ribosome modulation factor (*rmf*), which stores ribosomes by dimerization (75), was highly expressed under C- and N-stress under slow dilution rates.

We searched for genes that could provide a mechanistic underpinning for cell autoaggregation at high dilution rates. KT2440 can aggregate and form biofilms *via* the synthesis and export of a variety of polymers, including alginate, cellulose, exopolysaccharides, and lap proteins, many of which are controlled post-transcriptionally (76–80). In our experiments, genes involved in these pathways were not enriched in the faster dilution treatments; rather, many were more highly expressed in the slower dilution rate treatments or were specific to only one resource stress condition (Table S2). For example, the response regulator *cfcR* (PP_4959) and its post-transcriptional regulator *rsmE*, which control the level of c-di-GMP and modulate biofilm formation (81–83), were both more highly expressed at 0.12 h⁻¹. However, other genes involved in cell membrane biogenesis and flagellar synthesis were differentially expressed depending on the dilution rate. For

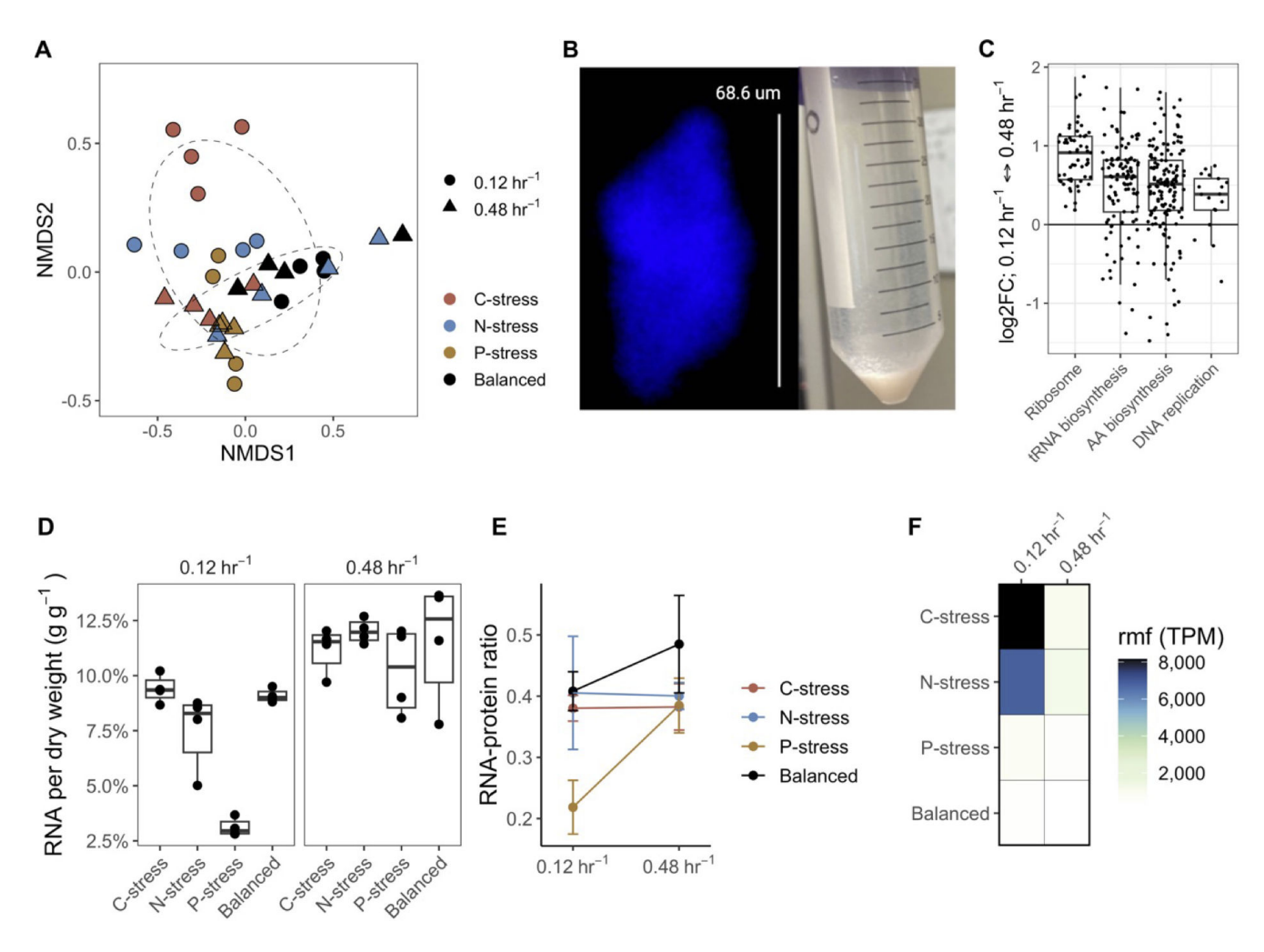


FIG 4 *P. putida* KT2440 physiology converges at fast dilution rates despite differences in resource stoichiometry, with specific changes in RNA. (A) Non-metric multidimensional scaling (NMDS) ordination based on Bray-Curtis dissimilatory of transcriptomes at different dilution rates and resource treatments. Circles represent the 75% confidence interval of each dilution rate. (B) A fluorescence microscopy image (with white scale bar) of a cell aggregate and photograph following culture removal from the chemostat showing flocculation at 0.48 h⁻¹. (C) Expression of genes involved in the pathways of ribosome synthesis, tRNAs, amino acids, and DNA replication as a function of dilution rate. Log2FC; log2FoldChange. (D) RNA content per dry weight. (E) The ratio of total RNA to total protein at different dilution rates and resource treatments. (F) Transcript expression (in transcripts per million, TPM) of the ribosome modulation factor (*rmf*).

example, *cfa* transcripts, responsible for the synthesis of cyclopropane fatty acids (CFAs), were enriched at slow dilution rates. Similarly, some gene clusters involved in flagellar synthesis, which are organized into at least 10 transcriptional units (84), were also more highly expressed at 0.12 h⁻¹. Altogether, mechanisms underlying the phenotypic transition from free-living to aggregation that accompanied increased dilution rate were not readily apparent from the transcriptional analyses. These results are consistent with previous studies working with *P. aeruginosa* that indicate that mechanisms controlling cell aggregation are not universal within a single strain and can be difficult to identify due to specific environmental conditions (85).

On balanced resource conditions

Finally, we compared the balanced medium condition (intended to represent optimal resource supply) against the various treatments designed to impose resource stress. Relative to the C, N, or P- stressed treatments, we found that cells in the balanced medium were enriched in transcripts for transposases, phage-associated genes, secretion systems, and the production of alginate, genes which were not highly expressed

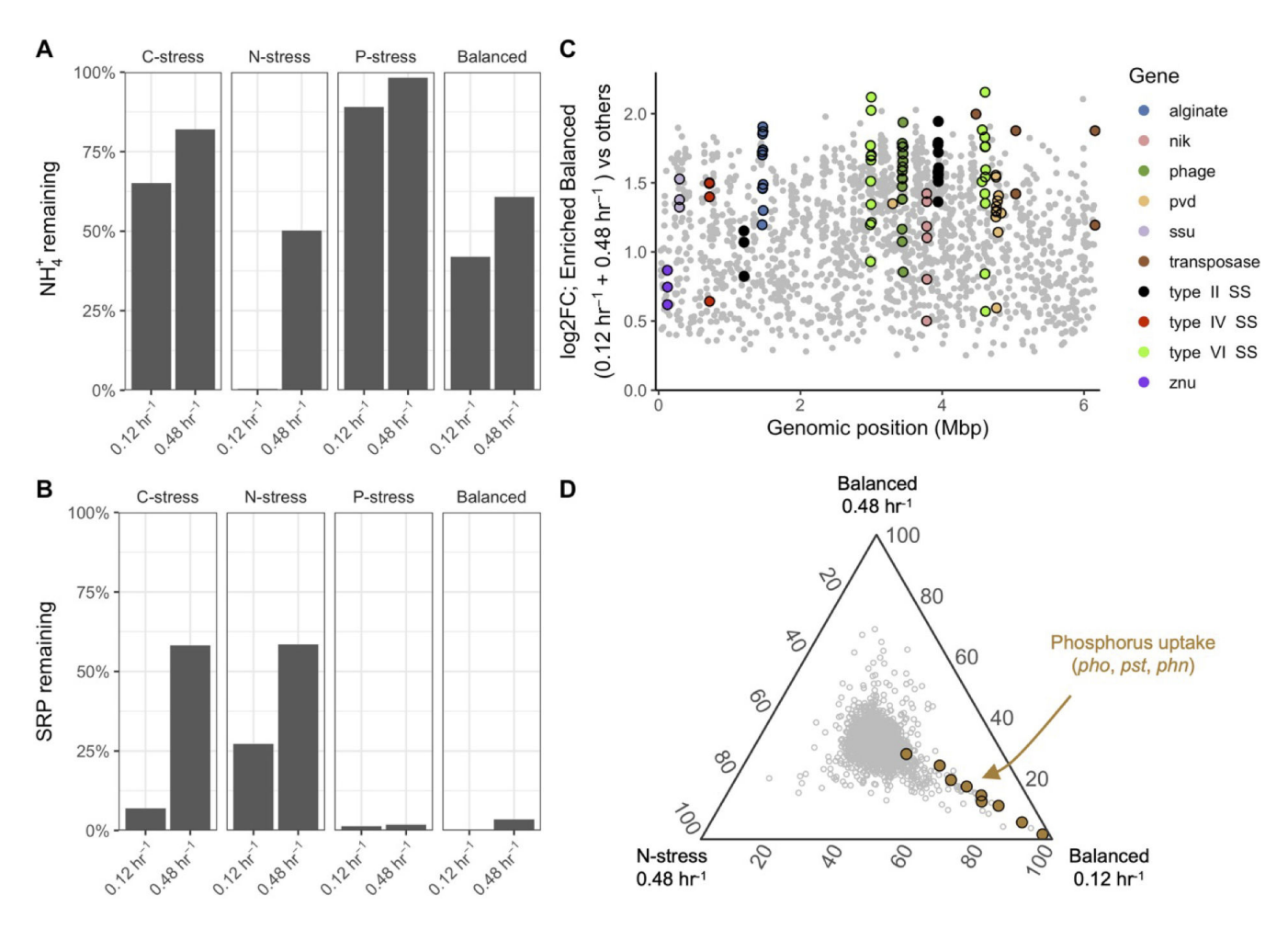


FIG 5 Cells supplied with Balanced medium C:N:P ratios appear phosphorus limited and express genes for the uptake of trace elements. (A and B) The proportion of the ammonium (NH_4^+) and soluble reactive phosphorus (SRP) remaining in the outflow as a function of nutrient stress and dilution rate. (C) Genes enriched (P < 0.05) under Balanced growth (0.12 h^{-1} and 0.48 h^{-1}) when compared against all other treatments. Genes of interest are shown in color and labeled. (D) Ternary plot comparing average relative percent transcript expression between Balanced (0.12 h^{-1} and 0.48 h^{-1}) and N-stress (0.48 h^{-1}) resource ratios, showing that transcriptomes under N-stress at high dilution rates are similar to those in cells grown under Balanced resource ratios. Each gray circle represents a gene.

overall but were nonetheless differentially abundant (Fig. 5; Table S10). Cells grown in the balanced treatments also had higher expression of transcripts for the uptake of micronutrients, including sulfonates (ssu), zinc (znu), nickel (nik), and the pyoverdine (pvd) operon that encodes for the production of siderophores and iron uptake. Taken together, these observations suggest that under optimal conditions, when cells are not as limited by C, N, and P, they may become limited by trace elements used as protein co-factors. Interestingly, many of these genes were also expressed by N-stressed cells at high dilution rates but not under C- and P-stress, highlighting similarities among cells under balanced growth at both dilution rates and N-stressed cells at high dilution rates (Fig. 5; Fig. S6; Table S11). Such findings are consistent with analyses of residual nutrients in the chemostats: at high dilution rates, both N-stressed and balanced chemostats had residual N and P, suggesting some other nutrient limited complete consumption of these elements in the chemostats.

DISCUSSION

Cells activate multiple pathways that transport and assimilate compounds containing the growth-limiting element

Here we evaluated the response of Pseudomonas putida KT2440 to changes in C, N, and P stoichiometry and dilution (growth) rate. Treatment-specific patterns of elemental stoichiometry and transcriptome expression were evident at slow dilution rates of 0.12 h⁻¹. One of the strongest responses to resource stress was the expression of regulatory pathways and transcripts related to the acquisition and assimilation of the growth-limiting element. This finding is consistent with previous work showing pseudomonads have a robust regulatory network that enables them to control their response to resource limitation (86–88). Under C-stress, KT2440 expressed crcZY, non-coding RNAs that sequester the Crc protein and release carbon catabolite repression of glucose assimilation (65-67, 89). Under N-stress, the gln operon, which regulates dozens of genes involved in N and C metabolism (26), was highly expressed. Our findings provide further support that the Crc and Ntr regulatory systems help regulate C:N biomass stoichiometry in Pseudomonas (26, 65, 67, 86, 87, 90, 91), especially under conditions of slow growth. We note that KT2440 also expressed transcripts for the acquisition of C, N, and P sources that were not supplied in the media. In our experiments, cells responded to C-stress by seeking to acquire not only glucose but also glycolate and glyoxylate. N-stressed cells activated pathways to acquire the ammonium supplied in the medium but also alternative forms of nitrogen, including nitrate, urea, and amino acids. Similarly, cells under P-stress expressed genes for the incorporation of not only phosphate but also phosphonates. Finally, both C- and N-stressed cells expressed transcripts for the uptake of alternative compounds containing both C and N moieties, such as amino acids and compatible solutes. Altogether, these observations show that KT2440 activates multiple pathways to acquire essential elements that are limiting to growth regardless of their form, including by recycling intracellular content, accessing metabolic byproducts, and scavenging dead extracellular material as cells decompose (7, 92, 93).

Different forms of resource stress induce specific changes in how carbon is partitioned between catabolic and anabolic pathways

Our findings also highlight how resource stress can induce changes in energy generation and carbon storage in slow-growing cells. For example, P stress resulted in increases in cellular C reserves, C:N and C:P ratios, and total lipids, coincident with elevated transcripts related to C metabolism and storage. By contrast, C-stress cells had lower cellular C and C:N and C:P ratios. These observations may be in part due to C storage as polyhydroxyalkanoates in P- and N-stressed cells. PHAs act as carbon and energy reservoirs to minimize energy spillage and may constitute up to 80% of cell dry weight under nutrient-limited conditions (94-101). Furthermore, our findings suggest that C-stressed cells maintained lower rates of respiration per ATP (or per cell), while P-stressed cells appeared to use less oxygen per unit dry weight despite greater rates of respiration per cell. We see evidence that underlying these changes in C storage and growth efficiency were modifications in respiratory electron transport pathways. KT2440 contains at least five terminal oxidases, each of which exhibits a unique redox potential, affinity for O₂, and ability to pump protons for ATP generation. These alternative pathways allow KT2440 to regulate respiration based on O₂ concentration, C source, growth phase, and nutrient limitation (98, 102-104). The cyo terminal oxidase, which was preferred at fast dilution rates in our experiments, acts as part of a global regulatory network that senses electron transport chain activity and influences the expression of hundreds of genes (102, 103, 105). At slow dilution rates, C-stressed cells used an aa₃-type oxidase preferentially to cyo, while P-stressed cells appear to rely more heavily on the cbb₃-1 oxidase. Oxidases of the aa₃-type can have higher proton-translocating efficiency than their cbb₃ counterparts (106-108). Hence, the aa₃ oxidase may function as an energy conservation mechanism under low C conditions (109). Changing

the terminal oxidase from cyo to aa₃ may have dual purposes for C-stressed cells: it could alter the expression of genes otherwise controlled by cyo and also optimize ATP generation in the face of decreased reductant flux and energy deficiency. Because we measured ATP pools, not fluxes, a valuable direction for future work would be to estimate ATP turnover under different types of resource stress (110, 111).

Cell auto-aggregation is a generic response to high dilution rate, regardless of resource limitation

One of the most visible phenomena we observed was autoaggregation of cells when grown at fast dilution rates. This switch in phenotype complicates the assessment of growth rate because flocculation could decouple dilution rate from cellular growth: aggregated and biofilm-associated cells have previously been shown to vary in growth rate, elemental ratios, and gene expression (104, 112, 113). The reasons for autoaggregation and biofilm formation can vary but can reflect a physiological mechanism that allows cells to persist in nutrient-enriched locations or to minimize cell stress (114, 115). Consistent with our study, previous work has shown that aggregative behavior by strains of P. putida occurs at high dilution rates (116–119). Similar aggregative behavior has also been reported in Enterococcus faecalis, Escherichia coli, Staphylococcus aereus, and P. aeruginosa during exponential growth (120, 121), with the latter growing predominantly as aggregates during conditions of fast growth (85, 122). Both P. putida and P. aeruginosa disperse from biofilms in response to starvation (29, 30, 122). Consistent with this observation, we found that at slow dilution rates, KT2440 differentially expressed transcripts for the production of cyclopropane fatty acids, ring-containing lipids synthesized in response to adverse conditions and during entry into the stationary phase (123-127), as well as flagellar transcripts that would be required for dispersal. Therefore, we hypothesize that KT2440 forms aggregates when growing rapidly under favorable conditions and disaggregates when resources become scarce. This physiological behavior may be both common (128) and important as bacteria approach μ_{max} , allowing cells to remain in a fixed, nutrient-rich location by preparing for surface attachment and biofilm formation. Further work will be needed to clarify the significance and mechanisms of this behavior in KT2440. This would require using near-instantaneous sampling protocols as aggregation responses can be transient.

P. putida cultured at high dilution rates converges on a common physiological phenotype regardless of media composition

Although cell aggregation complicates the use of dilution rate as a measure of growth rate in chemostats, we observed physiological changes that suggest KT2440 was growing faster at 0.48 h⁻¹ than at 0.12 h⁻¹. For example, while biomass elemental stoichiometry and transcriptome expression were flexible at the slow dilution rate, they were less variable and converged across treatments when the dilution rate approached μ_{max} . These findings are consistent with the observation that elemental stoichiometry of bacterial biomass varies depending on resource conditions, especially at slow growth, but converges at fast growth rates near a C:N:P of ~70:15:1 (9, 14). Similar trends have been reported for transcriptome composition, which shows a dependence on growth rate (129, 130) and convergence at fast growth (131). We also found that RNA became a larger proportion of cell biomass at faster dilution rates, consistent with previous studies that have documented positive relationships between cellular RNA pools and growth rate (71, 132–136). However, in our experiments, the strength of the RNA-growth rate relationship varied depending on resource stoichiometry. For example, increases in cellular RNA were most pronounced under P-stress, but more modest under C- or N-stress, in agreement with a previous study that found no change in RNA content as a function of growth rate under C-limitation in KT2440 (27). Bacterial P content can be highly flexible (137), suggesting differences in the fraction of active ribosomes and protein elongation rates may account for differences in RNA content (73, 138, 139). One mechanism for altering the number of active ribosomes is ribosomal hibernation via rmf

(140), a gene that was expressed by KT2440 here under C- and N-stress at slow growth. Elevated expression of rmf has been observed in C- and N-limited $E.\ coli\ (74)$, and rmf mutants show an inability to control ribosome abundance (141). The elevated pools of RNA that we observed at slow growth under C- and N- stress suggest that KT2440 maintains excess, stored ribosomes when P resources are abundant, permitting rapid increases in protein synthesis when limiting resources once again become available (5, 73, 135). Altogether, our data point to physiological changes that would be consistent with increases in growth rate as a function of dilution rate and that cell physiology is less variable as cells approach μ_{max} even under different resource ratios.

Changes in luxury gene expression may be one way cells respond to resource conditions

Finally, we explored the response of cells to more optimal resource conditions (Balanced medium treatment) where the N:P supply ratio matched the commonly observed cell biomass ratio of 16:1 (11, 33-35). Phenotypic and residual element concentrations indicated that cells in the Balanced medium behaved somewhat differently from the other treatments, suggesting a distinct physiology intermediate to N- or P-stress. Interestingly, we observed similar transcriptomic patterns in the Balanced treatments at both dilution rates and under N-stress at the fast dilution rate (0.48 h⁻¹). These findings were consistent with analyses of residual elements in the chemostats: at fast growth, both N-stressed and Balanced treatment chemostats had appreciable residual N and P. One explanation could be that as growth rates approach $\mu_{\text{max}\prime}$ residual concentrations of the limiting resource increase (142). Nevertheless, transcriptomic data may be consistent with the interpretation of a shift toward an alternative limiting resource at high growth rates. For example, shared transcripts specific to these three treatments (Balanced at 0.12 h⁻¹ and 0.48 h⁻¹, N stressed 0.48 h⁻¹) included those for the uptake of micronutrients, including the pyoverdine operon for the production of siderophores (pvd), sulfonates (ssu), zinc (znu), and nickel (nik), consistent with limitation by trace elements. We hypothesize that a dilution rate of 0.48 h⁻¹ may have relaxed N-stress but increased requirements for micronutrients such as sulfur, iron, or zinc. Future work should consider the role of growth rate on cellular micronutrient requirements (143). Interestingly, these three treatments also expressed luxury transcripts not required for growth in monoculture but which may provide an advantage in natural settings when competing with other organisms. Resource limitation can lead to downregulation of genes that potentially carry a fitness cost, including transposases (144), secretion systems (145), siderophores (146), and virulence traits (147, 148). We hypothesize that under fast growth when C, N, or P may be less limiting, luxury genes are expressed; however, downregulation of these genes, which are unnecessary to maintain growth and may carry a metabolic burden, could be one mechanism to deal with resource stress.

ACKNOWLEDGMENTS

Thank you to Adam Baumann and Sydni Racki for their technical expertise. We appreciate constructive feedback from members of the Rules of Life Team (Arizona State University, Oklahoma State University). Thank you to Mackenzie Gerringer and Bentley George for their helpful discussion. This work was funded by the US National Science Foundation (DEB-1930816 to J.J.E. and M.J.C.).

AUTHOR AFFILIATIONS

¹Flathead Lake Biological Station, University of Montana, Polson, Montana, USA

²Department of Biology, University of Copenhagen, Copenhagen, Denmark

³Division of Biological Sciences, University of Montana, Missoula, Montana, USA

⁴School of Biological Sciences, Georgia Institute of Technology, Atlanta, Georgia, USA

AUTHOR ORCIDs

Logan M. Peoples http://orcid.org/0000-0002-0163-2769
Jana Isanta-Navarro http://orcid.org/0000-0002-6168-4499

FUNDING

Funder	Grant(s)	Author(s)
National Science Foundation (NSF)	DEB-1930816	James J. Elser
		Matthew J. Church

AUTHOR CONTRIBUTIONS

Logan M. Peoples, Conceptualization, Data curation, Formal analysis, Investigation, Methodology, Visualization, Writing – original draft, Writing – review and editing | Jana Isanta-Navarro, Conceptualization, Investigation, Methodology, Writing – review and editing | Benedicta Bras, Conceptualization, Investigation, Methodology, Writing – review and editing | Brian K. Hand, Conceptualization, Investigation, Writing – review and editing | James J. Elser, Conceptualization, Funding acquisition, Investigation, Methodology, Project administration, Resources, Supervision, Writing – review and editing | Matthew J. Church, Conceptualization, Funding acquisition, Investigation, Methodology, Project administration, Resources, Supervision, Writing – original draft, Writing – review and editing

DATA AVAILABILITY

Transcriptomic data are publicly available under NCBI accession PRJNA1063263.

ADDITIONAL FILES

The following material is available online.

Supplemental Material

Supplemental Figures (mSystems00770-24-s0001.docx). Figures S1 to S7. **Supplemental Tables (mSystems00770-24-s0002.xlsx).** Tables S1 to S11.

REFERENCES

- Sterner RW, Elser JJ. 2003. Ecological stoichiometry: the biology of elements from molecules to the biosphere. Princeton University Press, Princeton.
- Moreno AR, Martiny AC. 2018. Ecological stoichiometry of ocean plankton. Ann Rev Mar Sci 10:43–69. https://doi.org/10.1146/annurevmarine-121916-063126
- Blackman FF. 1905. Optima and limiting factors. Ann Bot 19:281–296. https://doi.org/10.1093/oxfordjournals.aob.a089000
- Beardall J, Young E, Roberts S. 2001. Approaches for determining phytoplankton nutrient limitation. Aquat Sci 63:44–69. https://doi.org/ 10.1007/PL00001344
- Flynn KJ, Raven JA, Rees TAV, Finkel Z, Quigg A, Beardall J. 2010. Is the growth rate hypothesis applicable to microalgae? J Phycol 46:1–12. https://doi.org/10.1111/j.1529-8817.2009.00756.x
- Harder W, Dijkhuizen L. 1983. Physiological responses to nutrient limitation. Annu Rev Microbiol 37:1–23. https://doi.org/10.1146/ annurev.mi.37.100183.000245
- Merchant SS, Helmann JD. 2012. Elemental economy: microbial strategies for optimizing growth in the face of nutrient limitation. Adv Microb Physiol 60:91–210. https://doi.org/10.1016/B978-0-12-398264-3. 00002-4
- Terry KL, Laws EA, Burns DJ. 1985. Growth rate variation in the N:P requirement ratio of phytoplankton. J Phycol 21:323–329. https://doi. org/10.1111/j.0022-3646.1985.00323.x

- Makino W, Cotner JB, Sterner RW, Elser JJ. 2003. Are bacteria more like plants or animals? Growth rate and resource dependence of bacterial C:N:P stoichiometry. Funct Ecol 17:121–130. https://doi.org/10.1046/j. 1365-2435.2003.00712.x
- Godwin CM, Cotner JB. 2015. Stoichiometric flexibility in diverse aquatic heterotrophic bacteria is coupled to differences in cellular phosphorus quotas. Front Microbiol 6:159. https://doi.org/10.3389/ fmicb.2015.00159
- Godwin CM, Cotner JB. 2018. What intrinsic and extrinsic factors explain the stoichiometric diversity of aquatic heterotrophic bacteria? ISME J 12:598–609. https://doi.org/10.1038/ismej.2017.195
- Goldman JC, McCarthy JJ, Peavey DG. 1979. Growth rate influences on the chemical composition of phytoplankton in oceanic waters. Nature 279:210–215. https://doi.org/10.1038/279210a0
- Hillebrand H, Steinert G, Boersma M, Malzahn A, Meunier CL, Plum C, Ptacnik R. 2013. Goldman revisited: faster-growing phytoplankton has lower N:P and lower stoichiometric flexibility. Limnol Oceanogr58:2076–2088. https://doi.org/10.4319/lo.2013.58.6.2076
- Godwin CM, Whitaker EA, Cotner JB. 2017. Growth rate and resource imbalance interactively control biomass stoichiometry and elemental quotas of aquatic bacteria. Ecology 98:820–829. https://doi.org/10. 1002/ecy.1705
- Monod J. 1949. The growth of bacterial cultures. Annu Rev Microbiol 3:371–394. https://doi.org/10.1146/annurev.mi.03.100149.002103

10.1128/msystems.00770-24 **16**

- Spiers AJ, Buckling A, Rainey PB. 2000. The causes of *Pseudomonas* diversity. Microbiology (Reading) 146 (Pt 10):2345–2350. https://doi. org/10.1099/00221287-146-10-2345
- 17. Silby MW, Winstanley C, Godfrey SAC, Levy SB, Jackson RW. 2011. *Pseudomonas* genomes: diverse and adaptable. FEMS Microbiol Rev 35:652–680. https://doi.org/10.1111/j.1574-6976.2011.00269.x
- Saati-Santamaría Z, Baroncelli R, Rivas R, García-Fraile P. 2022. Comparative genomics of the genus *Pseudomonas* reveals host- and environment- specific evolution. Microbiol Spectr 10:e0237022. https://doi.org/10.1128/spectrum.02370-22
- Regenhardt D, Heuer H, Heim S, Fernandez DU, Strömpl C, Moore ERB, Timmis KN. 2002. Pedigree and taxonomic credentials of *Pseudomonas* putida strain KT2440. Environ Microbiol 4:912–915. https://doi.org/10. 1046/j.1462-2920.2002.00368.x
- Nakazawa T. 2002. Travels of a *Pseudomonas*, from Japan around the world. Environ Microbiol 4:782–786. https://doi.org/10.1046/j.1462-2920.2002.00310.x
- Dos Santos V, Heim S, Moore ERB, Strätz M, Timmis KN. 2004. Insights into the genomic basis of niche specificity of *Pseudomonas putida* KT2440. Environ Microbiol 6:1264–1286. https://doi.org/10.1111/j.1462-2920.2004.00734.x
- Kivisaar M. 2020. Narrative of a versatile and adept species *Pseudomo-nas putida*. J Med Microbiol 69:324–338. https://doi.org/10.1099/jmm.0.001137
- Nelson KE, Weinel C, Paulsen IT, Dodson RJ, Hilbert H, Martins dos Santos VAP, Fouts DE, Gill SR, Pop M, Holmes M, et al. 2002. Complete genome sequence and comparative analysis of the metabolically versatile *Pseudomonas putida* KT2440. Environ Microbiol 4:799–808. https://doi.org/10.1046/j.1462-2920.2002.00366.x
- Nogales Juan, Palsson BØ, Thiele I. 2008. A genome-scale metabolic reconstruction of *Pseudomonas putida* KT2440: iJN746 as a cell factory. BMC Syst Biol 2:79. https://doi.org/10.1186/1752-0509-2-79
- Nogales J, Mueller J, Gudmundsson S, Canalejo FJ, Duque E, Monk J, Feist AM, Ramos JL, Niu W, Palsson BO. 2020. High-quality genomescale metabolic modeling of *Pseudomonas putida* highlights its broad metabolic capabilities. Environ Microbiol 22:255–269. https://doi.org/ 10.1111/1462-2920.14843
- Hervás AB, Canosa I, Santero E. 2008. Transcriptome analysis of Pseudomonas putida in response to nitrogen availability. J Bacteriol 190:416–420. https://doi.org/10.1128/JB.01230-07
- van Duuren JBJH, Puchałka J, Mars AE, Bücker R, Eggink G, Wittmann C, Dos Santos VAPM. 2013. Reconciling in vivo and in silico key biological parameters of *Pseudomonas putida* KT2440 during growth on glucose under carbon-limited condition. BMC Biotechnol 13:93. https://doi.org/ 10.1186/1472-6750-13-93
- Mozejko-Ciesielska J, Pokoj T, Ciesielski S. 2018. Transcriptome remodeling of *Pseudomonas putida* KT2440 during mcl-PHAs synthesis: effect of different carbon sources and response to nitrogen stress. J Ind Microbiol Biotechnol 45:433–446. https://doi.org/10.1007/s10295-018-2042-4
- Gjermansen M, Ragas P, Sternberg C, Molin S, Tolker-Nielsen T. 2005. Characterization of starvation-induced dispersion in *Pseudomonas putida* biofilms. Environ Microbiol 7:894–906. https://doi.org/10.1111/j. 1462-2920.2005.00775.x
- Gjermansen M, Nilsson M, Yang L, Tolker-Nielsen T. 2010. Characterization of starvation-induced dispersion in *Pseudomonas putida* biofilms: genetic elements and molecular mechanisms. Mol Microbiol 75:815–826. https://doi.org/10.1111/j.1365-2958.2009.06793.x
- Díaz-Salazar C, Calero P, Espinosa-Portero R, Jiménez-Fernández A, Wirebrand L, Velasco-Domínguez MG, López-Sánchez A, Shingler V, Govantes F. 2017. The stringent response promotes biofilm dispersal in Pseudomonas putida. Sci Rep 7:18055. https://doi.org/10.1038/s41598-017-18518-0
- Kilham SS, Kreeger DA, Lynn SG, Goulden CE, Herrera L. 1998. COMBO: a defined freshwater culture medium for algae and zooplankton. Hydrobiologia 377:147–159. https://doi.org/10.1023/A:1003231628456
- Redfield AC. 1934. On the proportions of organic derivatives in sea water and their relation to the composition of plankton. James Johnstone Memorial Volume, University Press of Liverpool, 176-192, Liverpool, UK.

- 34. Redfield AC, Ketchum BH, Richards FA. 1963. The influence of organisms on the composition of sea-water, p 26–77. In Hill MN (ed), The composition of seawater: comparative and descriptive oceanography. The sea: ideas and observations on progress in the study of the seas. Vol. 2.
- Zimmerman AE, Allison SD, Martiny AC. 2014. Phylogenetic constraints on elemental stoichiometry and resource allocation in heterotrophic marine bacteria. Environ Microbiol 16:1398–1410. https://doi.org/10. 1111/1462-2920.12329
- Scott JT, Cotner JB, Lapara TM. 2012. Variable stoichiometry and homeostatic regulation of bacterial biomass elemental composition. Front Microbiol 3:42. https://doi.org/10.3389/fmicb.2012.00042
- Miller AW, Befort C, Kerr EO, Dunham MJ. 2013. Design and use of multiplexed chemostat arrays. J Vis Exp 72:e50262. https://doi.org/10. 3791/50262
- Dunham MJ, Kerr EO, Miller AW, Payen C. 2017. Chemostat culture for yeast physiology and experimental evolution. Cold Spring Harb Protoc 2017:pdb. https://doi.org/10.1101/pdb.top077610
- del Castillo T, Ramos JL, Rodríguez-Herva JJ, Fuhrer T, Sauer U, Duque E.
 2007. Convergent peripheral pathways catalyze initial glucose catabolism in *Pseudomonas putida*: genomic and flux analysis. J Bacteriol 189:5142–5152. https://doi.org/10.1128/JB.00203-07
- Tokic M, Hatzimanikatis V, Miskovic L. 2020. Large-scale kinetic metabolic models of *Pseudomonas putida* KT2440 for consistent design of metabolic engineering strategies. Biotechnol Biofuels 13:33. https:// doi.org/10.1186/s13068-020-1665-7
- Ferenci T. 2007. Bacterial physiology, regulation and mutational adaptation in a chemostat environment. Adv Microbiol Physiol 53:169– 229. https://doi.org/10.1016/S0065-2911(07)53003-1.
- Ojkic N, Serbanescu D, Banerjee S. 2019. Surface-to-volume scaling and aspect ratio preservation in rod-shaped bacteria. eLife 8. https://doi. org/10.7554/eLife.47033
- Karl DM, Dore JE, Hebel DV, Winn C. 1991. Procedures for particulate carbon, nitrogen, phosphorus and total mass analyses used in the US-JGOFS Hawaii ocean time-series program, p 71–77. In Hurd DC, Spencer DW (ed), Marine particles: analysis and characterization. American Geophysical Union, Washington, D.C. https://doi.org/10.1029/ GM063p0071.
- Gorokhova E, Kyle M. 2002. Analysis of nucleic acids in Daphnia: development of methods and ontogenetic variations in RNA-DNA content. J Plank Res 24:511–522. https://doi.org/10.1093/plankt/24.5.
- Kyle M, Watts T, Schade J, Elser JJ. 2003. A microfluorometric method for quantifying RNA and DNA in terrestrial insects. J Insect Sci 3:1. https://doi.org/10.1672/1536-2442(2003)003[0001:TMALBH]2.0.CO;2
- Gardner WS, Frez WA, Cichocki EA, Parrish CC. 1985. Micromethod for lipids in aquatic invertebrates. Limnol Oceanogr 30:1099–1105. https:// doi.org/10.4319/lo.1985.30.5.1099
- Lu Y, Ludsin SA, Fanslow DL, Pothoven SA. 2008. Comparison of three microquantity techniques for measuring total lipids in fish. Can J Fish Aquat Sci 65:2233–2241. https://doi.org/10.1139/F08-135
- Wagner ND, Lankadurai BP, Simpson MJ, Simpson AJ, Frost PC. 2015.
 Metabolomic differentiation of nutritional stress in an aquatic invertebrate. Physiol Biochem Zool 88:43–52. https://doi.org/10.1086/670637
- Bolger AM, Lohse M, Usadel B. 2014. Trimmomatic: a flexible trimmer for Illumina sequence data. Bioinformatics 30:2114–2120. https://doi. org/10.1093/bioinformatics/btu170
- Belda E, van Heck RGA, José Lopez-Sanchez M, Cruveiller S, Barbe V, Fraser C, Klenk H-P, Petersen J, Morgat A, Nikel PI, Vallenet D, Rouy Z, Sekowska A, Martins Dos Santos VAP, de Lorenzo V, Danchin A, Médigue C. 2016. The revisited genome of *Pseudomonas putida* KT2440 enlightens its value as a robust metabolic chassis. Environ Microbiol 18:3403–3424. https://doi.org/10.1111/1462-2920.13230
- 51. Langmead B, Salzberg SL. 2012. Fast gapped-read alignment with Bowtie 2. Nat Methods 9:357–359. https://doi.org/10.1038/nmeth.1923
- Li H, Handsaker B, Wysoker A, Fennell T, Ruan J, Homer N, Marth G, Abecasis G, Durbin R, 1000 Genome Project Data Processing Subgroup. 2009. The sequence alignment/map format and SAMtools. Bioinformatics 25:2078–2079. https://doi.org/10.1093/bioinformatics/btp352

- Liao Y, Smyth GK, Shi W. 2014. featureCounts: an efficient general purpose program for assigning sequence reads to genomic features. Bioinformatics 30:923–930. https://doi.org/10.1093/bioinformatics/ btt656
- Tatusova T, DiCuccio M, Badretdin A, Chetvernin V, Nawrocki EP, Zaslavsky L, Lomsadze A, Pruitt KD, Borodovsky M, Ostell J. 2016. NCBI prokaryotic genome annotation pipeline. Nucleic Acids Res. 44:6614– 6624. https://doi.org/10.1093/nar/gkw569
- Kanehisa M, Sato Y, Morishima K. 2016. BlastKOALA and GhostKOALA:
 KEGG tools for functional characterization of genome and metagenome sequences. J Mol Biol 428:726–731. https://doi.org/10.1016/j.jmb. 2015.11.006
- Ogata H, Goto S, Sato K, Fujibuchi W, Bono H, Kanehisa M. 1999. KEGG: Kyoto encyclopedia of genes and genomes. Nucl Acid Res27:29–34. https://doi.org/10.1093/nar/27.1.29
- Hamilton NE, Ferry M. 2018. ggtern: ternary diagrams using ggplot2. J Stat Software 87:1–17. https://doi.org/10.18637/jss.v087.c03
- Oksanen J, Blanchet FG, Kindt R, Legendre P, Minchin PR, O'hara RB, Simpson GL, Solymos P, Stevens MH, Wagner H, Oksanen MJ. 2013. Package 'vegan'. Community ecology package, version 2.9.
- Love MI, Huber W, Anders S. 2014. Moderated estimation of fold change and dispersion for RNA-seq data with DESeq2. Genome Biol. 15:550. https://doi.org/10.1186/s13059-014-0550-8
- Tenenbaum D, Maintainer B. 2023. KEGGREST: client-side REST access to the Kyoto encyclopedia of genes and genomes (KEGG). R package version 1.40.0. https://doi.org/doi:10.18129/B9.bioc.KEGGREST
- Wickham H. 2016. ggplot2. ggplot2: elegant graphics for data analysis.
 Springer-Verlag New York, Cham. Available from: http://link.springer.com/10.1007/978-3-319-24277-4
- 62. Bochdansky AB, Stouffer AN, Washington NN. 2021. Adenosine triphosphate (ATP) as a metric of microbial biomass in aquatic systems: new simplified protocols, laboratory validation, and a reflection on data from the literature. Limnol Ocean Methods 19:115–131. https://doi.org/10.1002/lom3.10409
- Delaquis PJ, Caldwell DE, Lawrence JR, McCurdy AR. 1989. Detachment of *Pseudomonas fluorescens* from biofilms on glass surfaces in response to nutrient stress. Microb Ecol 18:199–210. https://doi.org/10.1007/ RE02075808
- Sternberg C, Christensen BB, Johansen T, Toftgaard Nielsen A, Andersen JB, Givskov M, Molin S. 1999. Distribution of bacterial growth activity in flow-chamber biofilms. Appl Environ Microbiol 65:4108–4117. https:// doi.org/10.1128/AEM.65.9.4108-4117.1999
- Rojo F. 2010. Carbon catabolite repression in *Pseudomonas*: optimizing metabolic versatility and interactions with the environment. FEMS Microbiol Rev 34:658–684. https://doi.org/10.1111/j.1574-6976.2010. 00218.x
- Moreno R, Fonseca P, Rojo F. 2012. Two small RNAs, CrcY and CrcZ, act in concert to sequester the Crc global regulator in *Pseudomonas putida*, modulating catabolite repression. Mol Microbiol 83:24–40. https://doi. org/10.1111/j.1365-2958.2011.07912.x
- 67. Rosa R, Nogales J, Rojo F. 2015. The Crc/CrcZ-CrcY global regulatory system helps the integration of gluconeogenic and glycolytic metabolism in *Pseudomonas putida*. Environ Microbiol 17:3362–3378. https://doi.org/10.1111/1462-2920.12812
- Wanner BL. 1993. Gene regulation by phosphate in enteric bacteria. J Cell Biochem 51:47–54. https://doi.org/10.1002/jcb.240510110
- Franden MA, Jayakody LN, Li WJ, Wagner NJ, Cleveland NS, Michener WE, Hauer B, Blank LM, Wierckx N, Klebensberger J, Beckham GT. 2018.
 Engineering *Pseudomonas putida* KT2440 for efficient ethylene glycol utilization. Metab Eng 48:197–207. https://doi.org/10.1016/j.ymben. 2018.06.003
- Nikel Pl, Chavarría M, Fuhrer T, Sauer U, de Lorenzo V. 2015. Pseudomonas putida KT2440 strain metabolizes glucose through a cycle formed by enzymes of the Entner-Doudoroff, Embden-Meyerhof-Parnas, and pentose phosphate pathways. J Biol Chem 290:25920–25932. https:// doi.org/10.1074/jbc.M115.687749
- NEIDHARDT FC, MAGASANIK B. 1960. Studies on the role of ribonucleic acid in the growth of bacteria. Biochim Biophys Acta 42:99–116. https:// doi.org/10.1016/0006-3002(60)90757-5
- 72. Scott M, Gunderson CW, Mateescu EM, Zhang Z, Hwa T. 2010.
 Interdependence of cell growth and gene expression: origins and

- consequences. Science 330:1099–1102. https://doi.org/10.1126/science.1192588
- Li SHJ, Li Z, Park JO, King CG, Rabinowitz JD, Wingreen NS, Gitai Z. 2018. *Escherichia coli* translation strategies differ across carbon, nitrogen, and phosphorus limitation conditions. Nat Microbiol 3:939–947. https://doi.org/10.1038/s41564-018-0199-2
- Zhang D, Li SHJ, King CG, Wingreen NS, Gitai Z, Li Z. 2022. Global and gene-specific translational regulation in *Escherichia coli* across different conditions. PLoS Comput Biol 18:e1010641. https://doi.org/10.1371/ journal.pcbi.1010641
- Wada A, Igarashi K, Yoshimura S, Aimoto S, Ishihama A. 1995. Ribosome modulation factor: Stationary phase-specific inhibitor of ribosome functions from *Escherichia coli*. Biochem Biophys Res Commun 214:410–417. https://doi.org/10.1006/bbrc.1995.2302
- Martínez-Gil M, Yousef-Coronado F, Espinosa-Urgel M. 2010. LapF, the second largest *Pseudomonas putida protein*, contributes to plant root colonization and determines biofilm architecture. Mol Microbiol 77:549–561. https://doi.org/10.1111/j.1365-2958.2010.07249.x
- Nilsson M, Chiang WC, Fazli M, Gjermansen M, Givskov M, Tolker-Nielsen T. 2011. Influence of putative exopolysaccharide genes on Pseudomonas putida KT2440 biofilm stability. Environ Microbiol 13:1357–1369. https://doi.org/10.1111/j.1462-2920.2011.02447.x
- Gulez G, Altıntaş A, Fazli M, Dechesne A, Workman CT, Tolker-Nielsen T, Smets BF. 2014. Colony morphology and transcriptome profiling of Pseudomonas putida KT2440 and its mutants deficient in alginate or all EPS synthesis under controlled matric potentials. MicrobiologyOpen 3:457–469. https://doi.org/10.1002/mbo3.180
- López-Sánchez A, Leal-Morales A, Jiménez-Díaz L, Platero AI, Bardallo-Pérez J, Díaz-Romero A, Acemel RD, Illán JM, Jiménez-López J, Govantes F. 2016. Biofilm formation-defective mutants in *Pseudomonas putida*. FEMS Microbiol Lett 363:fnw127. https://doi.org/10.1093/femsle/fnw127
- Martínez-García E, Fraile S, Rodríguez Espeso D, Vecchietti D, Bertoni G, de Lorenzo V. 2020. Naked bacterium: emerging properties of a surfome-streamlined *Pseudomonas putida* strain. ACS Synth Biol 9:2477–2492. https://doi.org/10.1021/acssynbio.0c00272
- Ramos-González MI, Travieso ML, Soriano MI, Matilla MA, Huertas-Rosales Ó, Barrientos-Moreno L, Tagua VG, Espinosa-Urgel M. 2016. Genetic dissection of the regulatory network associated with high c-di-GMP levels in *Pseudomonas putida* KT2440. Front. Microbiol 7. https:// doi.org/10.3389/fmicb.2016.01093
- Huertas-Rosales Ó, Ramos-González MI, Espinosa-Urgel M. 2016. Selfregulation and interplay of Rsm family proteins modulate the lifestyle of *Pseudomonas putida*. Appl Environ Microbiol 82:5673–5686. https:// doi.org/10.1128/AEM.01724-16
- 83. Huertas-Rosales Ó, Romero M, Heeb S, Espinosa-Urgel M, Cámara M, Ramos-González MI. 2017. The *Pseudomonas putida* CsrA/RsmA homologues negatively affect c-di-GMP pools and biofilm formation through the GGDEF/EAL response regulator CfcR. Environ Microbiol 19:3551–3566. https://doi.org/10.1111/1462-2920.13848
- 84. Leal-Morales A, Pulido-Sánchez M, López-Sánchez A, Govantes F. 2022. Transcriptional organization and regulation of the *Pseudomonas putida* flagellar system. Environ Microbiol 24:137–157. https://doi.org/10.1111/1462-2920.15857
- Melaugh G, Martinez VA, Baker P, Hill PJ, Howell PL, Wozniak DJ, Allen RJ. 2023. Distinct types of multicellular aggregates in *Pseudomonas aeruginosa* liquid cultures. NPJ Biofilms Microbiomes 9:52. https://doi. org/10.1038/s41522-023-00412-5
- Li W, Lu CD. 2007. Regulation of carbon and nitrogen utilization by CbrAB and NtrBC two-component-systems in *Pseudomonas aeruginosa*. J Bacteriol 189:5413–5420. https://doi.org/10.1128/JB.00432-07
- 87. Naren N, Zhang XX. 2021. Role of a local transcription factor in governing cellular carbon/nitrogen homeostasis in *Pseudomonas fluorescens*. Nucleic Acids Res 49:3204–3216. https://doi.org/10.1093/nar/gkab091
- Moreno R, Rojo F. 2023. The importance of understanding the regulation of bacterial metabolism. Environ Microbiol 25:54–58. https:// doi.org/10.1111/1462-2920.16123
- Moreno R, Ruiz-Manzano A, Yuste L, Rojo F. 2007. The Pseudomonas putida Crc global regulator is an RNA binding protein that inhibits

10.1128/msystems.00770-24 **18**

- translation of the AlkS transcriptional regulator. Mol Microbiol 64:665–675. https://doi.org/10.1111/j.1365-2958.2007.05685.x
- Valentini M, García-Mauriño SM, Pérez-Martínez I, Santero E, Canosa I, Lapouge K. 2014. Hierarchical management of carbon sources is regulated similarly by the CbrA/B systems in *Pseudomonas aeruginosa* and *Pseudomonas putida*. Microbiology (Reading) 160:2243–2252. https://doi.org/10.1099/mic.0.078873-0
- 91. Sudarsan S, Dethlefsen S, Blank LM, Siemann-Herzberg M, Schmid A. 2014. The functional structure of central carbon metabolism in *Pseudomonas putida* KT2440. Appl Environ Microbiol 80:5292–5303. https://doi.org/10.1128/AEM.01643-14
- 92. Zimmer DP, Soupene E, Lee HL, Wendisch VF, Khodursky AB, Peter BJ, Bender RA, Kustu S. 2000. Nitrogen regulatory protein C-controlled genes of *Escherichia coli*: scavenging as a defense against nitrogen limitation. Proc Natl Acad Sci U S A 97:14674–14679. https://doi.org/10.1073/pnas.97.26.14674
- Moreno R, Martínez-Gomariz M, Yuste L, Gil C, Rojo F. 2009. The Pseudomonas putida Crc global regulator controls the hierarchical assimilation of amino acids in a complete medium: evidence from proteomic and genomic analyses. Proteomics 9:2910–2928. https://doi. org/10.1002/pmic.200800918
- Huijberts GNM, Eggink G. 1996. Production of poly(3-hydroyalkanoates) by Pseudomonas putida KT2442 in continuous culture. Appl Microbiol Biotechnol 46:233–239. https://doi.org/10.1007/s002530050810
- Durner R, Witholt B, Egli T. 2000. Accumulation of Poly[(R)-3-Hydroxyalkanoates] in *Pseudomonas oleovorans* during growth with octanoate in continuous culture at different dilution rates. Appl Environ Microbiol 66:3408–3414. https://doi.org/10.1128/AEM.66.8.3408-3414.2000
- Lee SY, Wong HH, Choi J, Lee SH, Lee SC, Han CS. 2000. Production of medium-chain-length polyhydroxyalkanoates by high-cell-density cultivation of *Pseudomonas putida* under phosphorus limitation. Biotechnol Bioeng 68:466–470. https://doi.org/10.1002/(SICI)1097-0290(20000520)68:4<466::AID-BIT12>3.0.CO;2-T
- Escapa IF, García JL, Bühler B, Blank LM, Prieto MA. 2012. The polyhydroxyalkanoate metabolism controls carbon and energy spillage in Pseudomonas putida. Environ Microbiol 14:1049–1063. https://doi.org/ 10.1111/j.1462-2920.2011.02684.x
- Poblete-Castro I, Escapa IF, Jäger C, Puchalka J, Lam CMC, Schomburg D, Prieto MA, Martins dos Santos VAP. 2012. The metabolic response of P. putida KT2442 producing high levels of polyhydroxyalkanoate under single- and multiple- nutrient-limited growth: Highlights from a multilevel omics approach. Microb Cell Fact 11:34. https://doi.org/10.1186/ 1475-2859-11-34
- 99. La Rosa R, de la Peña F, Prieto MA, Rojo F. 2014. The crc protein inhibits the production of polyhydroxyalkanoates in *Pseudomonas putida* under balanced carbon/nitrogen growth conditions. Environ Microbiol 16:278–290. https://doi.org/10.1111/1462-2920.12303
- Prieto A, Escapa IF, Martínez V, Dinjaski N, Herencias C, de la Peña F, Tarazona N, Revelles O. 2016. A Holistic view of polyhydroxyalkanoate metabolism in *Pseudomonas putida*. Environ Microbiol18:341–357. https://doi.org/10.1111/1462-2920.12760
- Mezzina MP, Manoli MT, Prieto MA, Nikel PI. 2021. Engineering native and synthetic pathways in *Pseudomonas putida* for the production of tailored polyhydroxyalkanoates. Biotechnol J 16:2000165. https://doi. org/10.1002/biot.202000165
- Dinamarca MA, Aranda-Olmedo I, Puyet A, Rojo F. 2003. Expression of the *Pseudomonas putida* OCT plasmid alkane degrdatation pathway is modulated by two different global control signals: evidence from continuous cultures. J Bacteriol 185:4772–4778. https://doi.org/10. 1128/JB.185.16.4772-4778.2003
- 103. Morales G, Ugidos A, Rojo F. 2006. Inactivation of the *Pseudomonas putida* cytochrome o ubiquinol oxidase leads to a significant change in the transcriptome and to increased expression of the CIO and cbb3-1 terminal oxidases. Environ Microbiol 8:1764–1774. https://doi.org/10. 1111/j.1462-2920.2006.01061.x
- Ugidos A, Morales G, Rial E, Williams HD, Rojo F. 2008. The coordinate regulation of multiple terminal oxidases by the *Pseudomonas putida* ANR global regulator. Environ Microbiol 10:1690–1702. https://doi.org/ 10.1111/i.1462-2920.2008.01586.x
- Dinamarca MA, Ruiz-Manzano A, Rojo F. 2002. Inactivation of the cytochrome o ubiquinol oxidase relieves catabolic repression of the

- Pseudomonas putida GPo1 alkane degradation pathway. J Bacteriol 184:3785–3793. https://doi.org/10.1128/JB.184.14.3785-3793.2002
- Lauraeus M, Wikström M. 1993. The terminal quinol oxidases of *Bacillus subtilis* have different energy conservation properties. J Biol Chem 268:11470–11473.
- 107. De JWL, Schepper M, Reijnders WNM, van SJ, Slotboom DJ, Warne A, Saraste M, Krab K, Finel M, Stouthamer AH, van der J. 1996. Structural and functional analysis of aa₃-type and cbb₃-type cytochrome c oxidases of *Paracoccus denitrificans* reveals significant differences in proton-pump design. Mol Microbiol 20:1247–1260. https://doi.org/10. 1111/j.1365-2958.1996.tb02644.x
- Pitcher RS, Watmough NJ. 2004. The bacterial cytochrome cbb₃ oxidases. Biochim Biophys Acta 1655:388–399. https://doi.org/10.1016/j.bbabio.2003.09.017
- 109. Kawakami T, Kuroki M, Ishii M, Igarashi Y, Arai H. 2010. Differential expression of multiple terminal oxidases for aerobic respiration in Pseudomonas aeruginosa. Environ Microbiol 12:1399–1412. https://doi. org/10.1111/j.1462-2920.2009.02109.x
- Karl DM, Bossard P. 1985. Measurement and significance of ATP and adenine nucleotide pool turnover in microbial cells and environmental samples. J Microbiol Methods 3:125–139. https://doi.org/10.1016/0167-7012(85)90040-5
- Ankenbauer A, Schäfer RA, Viegas SC, Pobre V, Voß B, Arraiano CM, Takors R. 2020. Pseudomonas putida KT2440 is naturally endowed to withstand industrial-scale stress conditions. Microb Biotechnol 13:1145–1161. https://doi.org/10.1111/1751-7915.13571
- 112. Sauer K, Camper AK. 2001. Characterization of phenotypic changes in *Pseudomonas putida* in response to surface-associated growth. J Bacteriol 183:6579–6589. https://doi.org/10.1128/JB.183.22.6579-6589. 2001
- Kragh K.N, Tolker-Nielsen T, Lichtenberg M. 2023. The non-attached biofilm aggregate. Commun Biol 6:898. https://doi.org/10.1038/s42003-023-05281-4
- Kragh Kasper N, Hutchison JB, Melaugh G, Rodesney C, Roberts AEL, Irie Y, Jensen PØ, Diggle SP, Allen RJ, Gordon V, Bjarnsholt T. 2016. Role of multicellular aggregates in biofilm formation. mBio 7:e00237. https:// doi.org/10.1128/mBio.00237-16
- Trunk T, Khalil HS, Leo JC. 2018. Bacterial autoaggregation. AIMS Microbiol 4:140–164. https://doi.org/10.3934/microbiol.2018.1.140
- Molin G. 1981. The impact of dilution rate and attached growth on steady-state characteristics of *Pseudomonas putida*. Eur J Appl Microbiol Biotechnol13:102–106. https://doi.org/10.1007/BF00499696
- Molin G, Nilsson I, Stenson-Holst L. 1982. Biofilm build-up of Pseudomonas putida in chemostats at different dilution rates. Eur J Appl Microbiol Biotechnol15:218–222. https://doi.org/10.1007/BF00499959
- Molin G. 1983. Measurement of the maximum specific growth rate in chemostat of *Pseudomonas* spp. with different abilities for biofilm formation. European J Appl Microbiol Biotechnol 18:303–307. https:// doi.org/10.1007/BF00500496
- Nilsson I, Dostálek M. 1984. Estimation of the biofilm formation ability of *Pseudomonas putida* in discrete samples from continuous culture. Appl Microbiol Biotechnol 20:183–188. https://doi.org/10.1007/ BF00253728
- Kragh KN, Alhede M, Rybtke M, Stavnsberg C, Jensen PØ, Tolker-Nielsen T, Whiteley M, Bjarnsholt T. 2018. The inoculation method could impact the outcome of microbiological experiments. Appl Environ Microbiol 84:e02264-17. https://doi.org/10.1128/AEM.02264-17
- Legner M, McMillen DR, Cvitkovitch DG. 2019. Role of dilution rate and nutrient availability in the formation of microbial biofilms. Front Microbiol 10:916. https://doi.org/10.3389/fmicb.2019.00916
- Schleheck D, Barraud N, Klebensberger J, Webb JS, McDougald D, Rice SA, Kjelleberg S. 2009. *Pseudomonas aeruginosa* PAO1 preferentially grows as aggregates in liquid batch cultures and disperses upon starvation. PLoS One 4:e5513. https://doi.org/10.1371/journal.pone. 0005513
- Cronan Jr JE. 1968. Phospholipid alterations during growth of *Escherichia coli*. J Bacteriol 95:2054–2061. https://doi.org/10.1128/jb.95. 6.2054-2061.1968
- 124. Wang A, Cronan JE Jr. 1994. The growth phase-dependent synthesis of cyclopropane fatty acids in *Escherichia coli* is the result of an RpoS(katF)-dependent promoter plus enzyme instability. Mol Microbiol 11:1009–1017. https://doi.org/10.1111/j.1365-2958.1994.tb00379.x
- Härtig C, Loffhagen N, Harms H. 2005. Formation of trans fatty acids is not involved in growth-linked membrane adaptation of Pseudomonas

10.1128/msystems.00770-24 **19**

- putida. Appl Environ Microbiol 71:1915–1922. https://doi.org/10.1128/AEM.71.4.1915-1922.2005
- 126. Muñoz-Rojas J, Bernal P, Duque E, Godoy P, Segura A, Ramos JL. 2006. Involvement of cyclopropane fatty acids in the response of *Pseudomonas putida* KT2440 to freeze-drying. Appl Environ Microbiol 72:472–477. https://doi.org/10.1128/AEM.72.1.472-477.2006
- Poger D, Mark AE. 2015. A ring to rule them all: the effect of cyclopropane fatty acids on the fluidity of lipid bilayers. J Phys Chem B 119:5487–5495. https://doi.org/10.1021/acs.jpcb.5b00958
- Cai YM. 2020. Non-surface attached bacterial aggregates: a ubiquitous third lifestyle. Front Microbiol 11:557035. https://doi.org/10.3389/ fmicb.2020.557035
- 129. Regenberg B, Grotkjaer T, Winther O, Fausbøll A, Akesson M, Bro C, Hansen LK, Brunak S, Nielsen J. 2006. Growth-rate regulated genes have profound impact on interpretation of transcriptome profiling in Saccharomyces cerevisiae. Genome Biol. 7:R107. https://doi.org/10. 1186/gb-2006-7-11-r107
- Matsumoto Y, Murakami Y, Tsuru S, Ying BW, Yomo T. 2013. Growth rate-coordinated transcriptome organization in bacteria. BMC Genomics 14:808. https://doi.org/10.1186/1471-2164-14-808
- Hua Q, Yang C, Oshima T, Mori H, Shimizu K. 2004. Analysis of gene expression in *Escherichia coli* in response to changes of growth-limiting nutrient in chemostat cultures. Appl Environ Microbiol 70:2354–2366. https://doi.org/10.1128/AEM.70.4.2354-2366.2004
- Kjeldgaard NO, Kurland CG. 1963. The distributions of soluble and ribosomal RNA as a function of growth rate. J Mol Biol6:341–348. https://doi.org/10.1016/S0022-2836(63)80093-5
- SCHAECHTER M, MAALOE O, KJELDGAARD NO. 1958. Dependency on medium and temperature of cell size and chemical composition during balanced growth of Salmonella typhimurium. J Gen Microbiol 19:592– 606. https://doi.org/10.1099/00221287-19-3-592
- 134. Elser JJ, Sterner RW, Gorokhova E, Fagan WF, Markow TA, Cotner JB, Harrison JF, Hobbie SE, Odell GM, Weider LW. 2000. Biological stoichiometry from genes to ecosystems. Ecology Letters 3:540–550. https://doi.org/10.1111/j.1461-0248.2000.00185.x
- Bremer H, Dennis PP. 2008. Modulation of chemical composition and other parameters of the cell at different exponential growth rates. EcoSal Plus 3. https://doi.org/10.1128/ecosal.5.2.3
- Isanta-Navarro J, Prater C, Peoples LM, Loladze I, Phan T, Jeyasingh PD, Church MJ, Kuang Y, Elser JJ. 2022. Revisiting the growth rate hypothesis: towards a holistic stoichiometric understanding of growth. Ecol Lett 25:2324–2339. https://doi.org/10.1111/ele.14096
- Godwin CM, Cotner JB. 2015. Aquatic heterotrophic bacteria have highly flexible phosphorus content and biomass stoichiometry. ISME J 9:2324–2327. https://doi.org/10.1038/ismej.2015.34

- Dai X, Zhu M, Warren M, Balakrishnan R, Patsalo V, Okano H, Williamson JR, Fredrick K, Wang Y-P, Hwa T. 2017. Reduction of translating ribosomes enables *Escherichia coli* to maintain elongation rates during slow growth. Nat Microbiol 2:16231. https://doi.org/10.1038/ nmicrobiol.2016.231
- Fessler M, Gummesson B, Charbon G, Svenningsen SL, Sørensen MA.
 2020. Short-term kinetics of rRNA degradation in *Escherichia coli* upon starvation for carbon, amino acid or phosphate. Mol Microbiol 113:951–963. https://doi.org/10.1111/mmi.14462
- 140. Yoshida H, Maki Y, Kato H, Fujisawa H, Izutsu K, Wada C, Wada A. 2002. The ribosome modulation factor (RMF) binding site on the 100S ribosome of *Escherichia coli*. J Biochem 132:983–989. https://doi.org/10.1093/oxfordjournals.jbchem.a003313
- Sebastian H, Finkel SE. 2022. Absence of ribosome modulation factor alters growth and competitive fitness of *Escherichia coli*. Microbiol Spectr 10:e0223921. https://doi.org/10.1128/spectrum.02239-21
- Smith HL, Waltman P. 1995. The theory of the chemostat. In The theory
 of the chemostat: dynamics of microbial competition. Cambridge
 University Press.
- 143. Kaspari M. 2021. The invisible hand of the periodic table: how micronutrients shape ecology. Annu Rev Ecol Evol Syst 52:199–219. https://doi.org/10.1146/annurev-ecolsys-012021-090118
- 144. Steffen MM, Dearth SP, Dill BD, Li Z, Larsen KM, Campagna SR, Wilhelm SW. 2014. Nutrients drive transcriptional changes that maintain metabolic homeostasis but alter genome architecture in *Microcystis*. ISME J 8:2080–2092. https://doi.org/10.1038/ismej.2014.78
- 145. Decanio MS, Landick R, Haft RJF. 2013. The non-pathogenic Escherichia coli strain W secretes SsIE via the virulence-associated type II secretion system beta. BMC Microbiol 13:130. https://doi.org/10.1186/1471-2180-13-130
- Sexton DJ, Schuster M. 2017. Nutrient limitation determines the fitness of cheaters in bacterial siderophore cooperation. Nat Commun 8:230. https://doi.org/10.1038/s41467-017-00222-2
- Browne P, Barret M, O'Gara F, Morrissey JP. 2010. Computational prediction of the Crc regulon identifies genus-wide and species-specific targets of catabolite repression control in *Pseudomonas* bacteria. BMC Microbiol 10:300. https://doi.org/10.1186/1471-2180-10-300
- Linares JF, Moreno R, Fajardo A, Martínez-Solano L, Escalante R, Rojo F, Martínez JL. 2010. The global regulator Crc modulates metabolism, susceptibility to antibiotics and virulence in *Pseudomonas aeruginosa*. Environ Microbiol 12:3196–3212. https://doi.org/10.1111/j.1462-2920. 2010.02292.x